



## UTLS water vapour from SCIAMACHY limb measurements V3.01 (2002–2012)

K. Weigel<sup>1</sup>, A. Rozanov<sup>1</sup>, F. Azam<sup>1</sup>, K. Bramstedt<sup>1</sup>, R. Damadeo<sup>2</sup>, K.-U. Eichmann<sup>1</sup>, C. Gebhardt<sup>1,a</sup>, D. Hurst<sup>3,4</sup>, M. Kraemer<sup>5</sup>, S. Lossow<sup>6</sup>, W. Read<sup>7</sup>, N. Spelten<sup>5</sup>, G. P. Stiller<sup>6</sup>, K. A. Walker<sup>8</sup>, M. Weber<sup>1</sup>, H. Bovensmann<sup>1</sup>, and J. P. Burrows<sup>1</sup>

<sup>1</sup>Institute of Environmental Physics – IUP, University of Bremen, Bremen, Germany

<sup>2</sup>NASA Langley Research Center, Hampton, Virginia, USA

<sup>3</sup>Cooperative Institute for Research in Environmental Sciences, University of Colorado, Boulder, Colorado, USA

<sup>4</sup>Global Monitoring Division, NOAA Earth System Research Laboratory, Boulder, Colorado, USA

<sup>5</sup>Forschungszentrum Jülich GmbH, Institute for Energy and Climate Research – Stratosphere IEK-7, Jülich, Germany

<sup>6</sup>Karlsruhe Institute of Technology – KIT, Institute for Meteorology and Climate Research – IMK, Karlsruhe, Germany

<sup>7</sup>Jet Propulsion Laboratory, California Institute of Technology, Pasadena, California, USA

<sup>8</sup>Department of Physics, University of Toronto, Toronto, Canada

<sup>a</sup>now at: Deutsches Zentrum für Luft- und Raumfahrt e.V. – DLR, Earth Observation Center, Bremen, Germany

Correspondence to: K. Weigel (weigel@iup.physik.uni-bremen.de)

Received: 8 May 2015 – Published in Atmos. Meas. Tech. Discuss.: 31 July 2015

Revised: 9 December 2015 – Accepted: 14 December 2015 – Published: 18 January 2016

**Abstract.** The SCanning Imaging Absorption spectroMeter for Atmospheric CHartography (SCIAMACHY) aboard the Envisat satellite provided measurements from August 2002 until April 2012. SCIAMACHY measured the scattered or direct sunlight using different observation geometries. The limb viewing geometry allows the retrieval of water vapour at about 10–25 km height from the near-infrared spectral range (1353–1410 nm). These data cover the upper troposphere and lower stratosphere (UTLS), a region in the atmosphere which is of special interest for a variety of dynamical and chemical processes as well as for the radiative forcing. Here, the latest data version of water vapour (V3.01) from SCIAMACHY limb measurements is presented and validated by comparisons with data sets from other satellite and in situ measurements. Considering retrieval tests and the results of these comparisons, the V3.01 data are reliable from about 11 to 23 km and the best results are found in the middle of the profiles between about 14 and 20 km. Above 20 km in the extra tropics V3.01 is drier than all other data sets. Additionally, for altitudes above about 19 km, the vertical resolution of the retrieved profile is not sufficient to resolve signals with a short vertical structure like the tape recorder. Below 14 km, SCIAMACHY water vapour V3.01 is wetter than most col-

located data sets, but the high variability of water vapour in the troposphere complicates the comparison. For 14–20 km height, the expected errors from the retrieval and simulations and the mean differences to collocated data sets are usually smaller than 10 % when the resolution of the SCIAMACHY data is taken into account. In general, the temporal changes agree well with collocated data sets except for the Northern Hemisphere extratropical stratosphere, where larger differences are observed. This indicates a possible drift in V3.01 most probably caused by the incomplete treatment of volcanic aerosols in the retrieval. In all other regions a good temporal stability is shown. In the tropical stratosphere an increase in water vapour is found between 2002 and 2012, which is in agreement with other satellite data sets for overlapping time periods.

## 1 Introduction

The upper troposphere and lower stratosphere (UTLS) is the region close to the tropopause. Here, a minimum in water vapour mixing ratios, the hygropause, is located (see e.g. Gettelman et al., 2011). Due to these low water vapour mixing ratios, which are often close to the detection limit of the instruments, it is challenging to measure water vapour at these altitudes, both for in situ instruments (see e.g. Weinstock et al., 2009; Rollins et al., 2014) and satellites (see e.g. Hegglin et al., 2013). However, the amount of water vapour in this region plays a key role in several atmospheric processes. The water vapour in the UTLS has a strong influence on the radiative budget of the atmosphere (e.g. Forster and Shine, 2002; Solomon et al., 2010; Riese et al., 2012). In the tropopause region, the incomplete knowledge about water vapour leads to major uncertainties in the assessment of atmospheric radiative forcing and hence global warming (Kunz et al., 2013). Therefore, it is important to monitor and understand changes in the water vapour amount in the UTLS.

The main sources for water vapour in the stratosphere are methane oxidation and the transport through the tropical tropopause layer (TTL). The methane increase in the stratosphere can only explain part of the water vapour changes (e.g. Rosenlof et al., 2001; Rohs et al., 2006). Another important contribution is the transport through the TTL, which plays a significant role for the amount of water vapour and its changes in the lower stratosphere. This transport depends to a large extent on the temperatures in the TTL (e.g. Fueglistaler and Haynes, 2005). One of the prominent signals in the natural variability of water vapour is the tape recorder effect in the tropical lower stratosphere, which is caused by the annual cycle in the TTL temperatures (Mote et al., 1996).

There are few long time series of more than a decade of measurements in the UTLS regions; see e.g. Hurst et al. (2011) for more details. Such time series are needed to identify trends in the observed atmospheric variables (Weatherhead et al., 1998) and distinguish them from periodic long-term variability. Only global and long-term observations can provide a comprehensive picture of water vapour in the UTLS. The SCanning Imaging Absorption spectroMeter for Atmospheric CHartographY (SCIAMACHY) (Burrrows et al., 1995), an instrument on the European satellite Envisat, provided measurements from August 2002 until the sudden end of the Envisat operation in April 2012, covering nearly 1 decade (Gottwald and Bovensmann, 2011). SCIAMACHY operated in three different viewing geometries: limb, nadir, and occultation (Bovensmann et al., 1999). This study will focus on SCIAMACHY limb measurements; comparisons with SCIAMACHY occultation measurements will also be presented. Limb measurements of scattered solar radiation in the near-infrared (1353–1410 nm) are used to retrieve water vapour profiles in the UTLS. The data cover the altitude range between about 10 and 25 km with a vertical sampling of about 3.3 km and provide near-global coverage

during daylight. Here, we present the data version V3.01 and evaluate its reliability by simulations and comparisons to in situ measurements and other satellite data sets.

## 2 Data set V3.01

### 2.1 Water vapour retrieval

The IUP (Institut für Umweltphysik, English: Institute of Environmental Physics) Bremen limb water vapour retrieval algorithm V3.01 follows the retrieval concept presented in Rozanov et al. (2011a) for V3. In the following, this setup is summarized and several small changes, which are introduced in V3.01 compared to V3, are explained. These changes include an improved aerosol correction, modifications to accelerate the retrieval convergence, a new level 1 (L1) data version, and a different choice of pressure and temperature fields.

As explained in Rozanov et al. (2011a) the retrieval is based on the optimal-estimation-type approach (Rodgers, 2000) with first-order Tikhonov constraint. A Gauss–Newton iterative scheme (Rodgers, 2000) is applied to account for the non-linearity of the inverse problem. SCIAMACHY limb measurements at the tangent heights between about 11 and 25 km are used. At each tangent height the spectrum is normalized by the solar spectrum measured in the same orbit. A variable correction for wavelength misalignments is applied before the retrieval using the FORTRAN library package GALAHAD V2.0 (Gould et al., 2003) for both limb and solar spectrum. Only the resulting differential absorption structures are evaluated to reduce the influence of aerosols and surface albedo. The retrieval uses logarithms of the measured radiation and of the water vapour number densities. In addition to water vapour, a fit for methane is included as well as the surface albedo and a scaling factor for the stratospheric aerosol profile, which is retrieved from SCIAMACHY data in a preceding step. Also, the tropospheric contribution parameter, a parameter describing the contribution of the water vapour below the level of the retrieval (10 km) is fitted. This contribution depends on both the amount of water vapour below the measurement heights and the effective surface elevation (which can be the real earth surface or an elevated altitude due to opaque clouds). These two components are not fitted simultaneously. During the first iterations (at least four and as many as necessary to limit the changes of the effective surface elevation to less than 500 m in two consecutive iterations) the tropospheric contribution parameter describes the effective surface elevation. A scaling factor for the tropospheric water vapour profile is determined in further iterations.

SCIATRAN V3.1 is used as a radiative transfer model (Rozanov et al., 2014). The limb radiance is calculated including the multiple scattering contribution. For the multiple scattering, the combined differential-integral approach is ap-

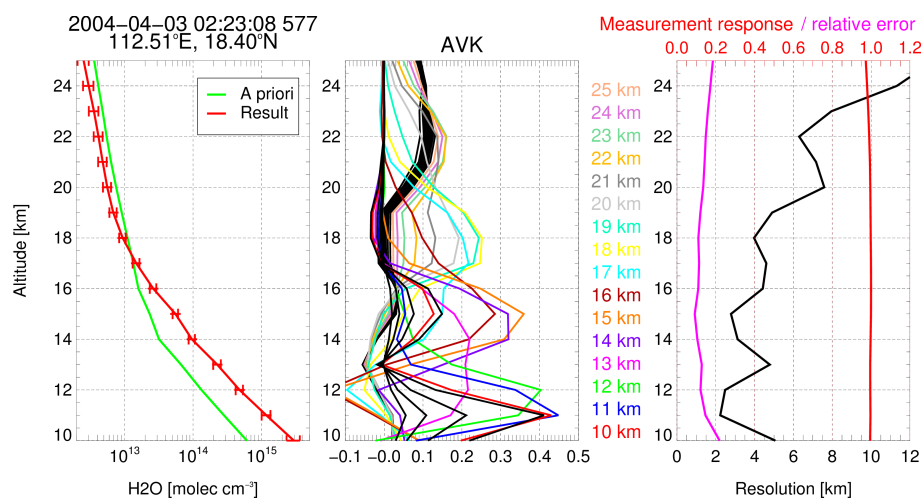


**Figure 1.** Left panel: an example of a water vapour profile resulting from the retrieval. Middle panel: corresponding averaging kernels. The colour marks the rows of the AVK matrix for heights between 10 and 25 km; rows for heights above and below are displayed in black. Right panel: vertical resolution (black), measurement response (red), and relative error of the retrieved profile (pink, top axis applies).

plied using a pseudo-spherical model with solar zenith angle and viewing angles set according to the spherical ray tracing. This is done for each point along the line of sight (LOS). Weighting functions are calculated with the single scattering approximation apart from the ones for the tropospheric contribution parameter, surface albedo, and stratospheric aerosols, where a perturbation method is used. The single scattering contribution and the integration of both contributions is calculated in a fully spherical atmosphere. The refraction is taken into account during ray tracing. The forward model uses the correlated- $k$  distribution technique (Buchwitz et al., 2000) with ESFT (exponential-sum fitting of transmissions) coefficients calculated using the HITRAN 2008 database (Rothman et al., 2009) including updates for water vapour lines which were provided on the HITRAN home page until 2010. For ESFT, 10 coefficients are pre-calculated at 20 pressure and 9 temperature grid points (case P20 T9 C10) in 0.2 nm spectral bins. As shown in Azam et al. (2012), these coefficients are sufficient below about 28 km height (see their Fig. 10 result for P20 T9 C10). They are therefore used for the limb retrieval in contrast to the lunar occultation retrieval, which covers a larger height range and requires a larger number of coefficients, which increases the calculation time.

The signal-to-noise ratio (SNR) of the sun-normalized radiances is calculated from the spectral residuals multiplied by a factor of 1.5 after the wavelength shift correction is applied. The SNR obtained in this manner is not identical with the instrumental L1 SNR but does include additional, partly systematic errors, which are part of the residual. The multiplication by 1.5 shall account for these systematic features in the residuals, which should not be part of the noise error. The SNR is usually between 400 and 700. It is largest for lower altitudes.

The retrieval unit for the water vapour in SCIAMACHY is the logarithm of number density. In addition the results are provided in a volume mixing ratio calculated using ECMWF (European Centre for Medium-range Weather Forecast) pressure and temperature fields. ECMWF Interim reanalysis pressure and temperature fields are used in V3.01 instead of ECMWF operational analysis used in V3. The ECMWF reanalysis is calculated with a consistent model version while the model for the ECMWF analysis data changes without re-processing, e.g. in 2006 a finer model grid was introduced. The different ECMWF fields had, however, only a minor influence on the resulting water vapour profiles.

The left panel of Fig. 1, shows a SCIAMACHY water vapour profile as a retrieval example together with the a priori profile. The retrieval is run on a grid between 0 and 60 km height, the grid step is 1 km between 6 and 36 km and coarser above and below. The error bars show the retrieval error calculated from the residuals. As a priori profiles, the trace gas vertical distributions according to the 1976 US standard atmosphere model are used for methane and water vapour. The a priori error is set to 300 % for water vapour and 30 % for methane. For water vapour, the smoothness coefficient for the first-order Tikhonov constraint increases linearly from 5 at 10 km to 10 at 30 km, while a smoothness coefficient of 1 is used at all altitude layers for methane (see Rozanov et al., 2011a for details). The averaging kernels (AVKs) belonging to the water vapour profile are shown in the middle panel of Fig. 1. The rows of the AVK show the sensitivity of the retrieval result on the true state (Rodgers, 2000). One colour always marks a row of the AVK matrix for water vapour at one altitude of the retrieval grid between 10 and 25 km; the rows of the AVK matrix for altitudes below and above are displayed in black. The maxima of these AVK rows cluster at certain heights showing where the informa-

tion for the retrieval result comes from. These clusters result from a retrieval grid which is denser than the vertical sampling. For SCIAMACHY limb measurements, the vertical sampling is about 3.3 km. The vertical field of view (FOV) is about 2.5 km. Especially the lower part of the profile is influenced by the refraction of the LOS in the Earth's atmosphere. Therefore, the distance between two tangent points can be larger than 3.3 km. In combination with the regularization, the extent of the FOV, and the vertical sampling yield the height-dependent resolution of the retrieved water vapour profile, shown in the right panel of Fig. 1. As in Hoffmann et al. (2008), it is calculated as reciprocal values of the diagonal elements of the averaging kernel matrix multiplied by the retrieval grid spacing. This method is based on the concept of information density (Purser and Huang, 1993) and yields comparable results to the Backus and Gilbert approach (Backus and Gilbert, 1970) used e.g. in Rozanov et al. (2011a) for V3 of the water vapour from SCIAMACHY limb measurements.

The lowest part of the profile shows the best vertical resolution of about 2.5 km. Here, the result is mainly influenced by one measurement, therefore resolutions close to the FOV size are possible. The resolution becomes coarser with increasing height and between the measurement heights at about 11.6, 15, 18.3, 21.6, and 24.9 km, where local minima in the vertical resolution are seen. For all SCIAMACHY limb profiles the measurements are taken at about the same heights, leading to a systematic variation of the resolution with altitude in the data set. The coarser resolution at higher altitudes is caused by a lower SNR combined with the increased smoothness coefficient. At 22 km, the resolution is clearly coarser than the 2.5 km FOV width, also at the grid point closest to measurement height, because due to the regularization and the lower SNR at 22 km, this height is influenced by the measurement below at about 18 km. In addition, the right panel of Fig. 1 shows the integral of the AVK rows ("measurement response"). It is a rough measure of the influence of the data rather than the a priori value on the retrieval result (Rodgers, 2000). It shows that the magnitude of the a priori value has no large influence on the result. Nevertheless, the shape of the a priori profile influences the result due to the smoothing constraint.

The calibration settings and the spectral interval (1353–1410 nm) remain the same as in Rozanov et al. (2011a). One of the changes in V3.01 compared to V3 is that L1 data versions V7.03 and 7.04 of SCIAMACHY are used instead of V6.03. The change of the L1 data version was necessary because V6.03 is not provided for data after September 2010. The differences between V6.03 and V7.03 include a small change in the calculation of instrument pointing and wavelength calibration. Additionally, there was a change in the consolidation of L1 V7.04 (from U to W). For data of V7.04U, problems with the assignment of the solar spectrum were reported. However, tests have shown that the differences between V7.03 and V7.04U/W are usually negligible.

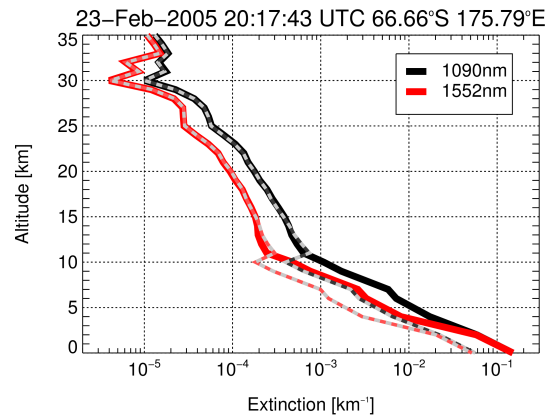


**Figure 2.** Aerosol extinction profiles for V3 (dashed lines) and V3.01 (solid lines) for the two wavelengths used in the aerosol retrieval (1090 nm black and grey line, 1552 nm red and orange line).

Due to the long data processing time it was not possible to provide the complete time series with a consistent L1 version.

In contrast to V3, the a priori values for tropospheric contribution parameter, surface albedo, and stratospheric aerosol scaling are not replaced after each iterative step. This change allows a faster retrieval convergence for V3.01. The iterative process, which is limited to a maximum of 12 steps, is stopped after one of the following convergence criteria is reached. The first criterion is that the relative change of the root mean square (RMS) of the fit residual  $RMS_{i-1}/RMS_i - 1$  is lower than  $10^{-3}$ . The second criterion is the relative change of the retrieved parameters with a threshold of 0.01, which is defined as the maximum relative change in the number densities between 12 and 23 km. Convergence is reached for about 73 % of all retrieved profiles; only these are included in the data set. Non-converging profiles are mainly due to cases where the SNR is low or where the retrieval of the tropospheric contribution parameter and the albedo is difficult and they are more frequent at high northern and southern latitudes.

In Rozanov et al. (2011a) the importance of the aerosol correction for the SCIAMACHY water vapour retrieval was highlighted. For both data versions, an aerosol retrieval is run between 12 and 35 km prior to the water vapour retrieval and the resulting aerosol profile is used as input. Further tests showed that not only the stratospheric aerosol within the LOS, but also the aerosols below the retrieval altitudes influence the result. In V3 the a priori profile was used below 12 km. Large differences between the a priori aerosol profile and the retrieved stratospheric aerosol led to large vertical gradients between 10 and 12 km. Figure 2 shows an example of an aerosol extinction profile for V3.0 together with the corresponding one for V3.01. In V3.01, the a priori aerosol extinction profile below 12 km is scaled to match the retrieved

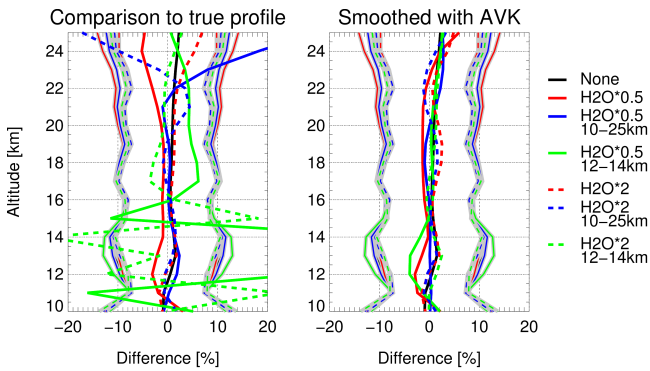


**Figure 3.** End-to-end tests for an unperturbed atmosphere (black lines) and for different perturbations of the water vapour profile (coloured solid and dashed lines). All lines show the difference between the retrieved and reference profiles, divided by the reference. The coloured solid lines show the error for profiles with halved water vapour for the complete profile (0–60 km, red), the retrieval heights (10–25 km, blue), and a 2 km layer (12–14 km, green). The coloured dashed lines show the differences for doubled water vapour profiles in the same height ranges as for half of the water vapour. The left panel shows the comparison between the retrieval result and the original water vapour profile. In the right panel the original profile is smoothed with the AVK resulting from the retrieval to exclude differences caused by the resolution. The lines underlaid with grey shading show the retrieval precision based on a constant SNR of 500.

profile at 12 km using a first-order Tikhonov smoothing up to 12 km.

## 2.2 End-to-end tests

To evaluate the reliability of the retrieval, end-to-end tests are performed. Here either an unperturbed (standard) or perturbed atmosphere is used to simulate the limb radiances that SCIAMACHY would measure with a given observation geometry. These observation geometries change along the orbit, therefore the corresponding regions are labelled in the following figures. Different observation geometries from selected measured SCIAMACHY profiles for Northern Hemisphere (NH) and Southern Hemisphere (SH) mid-latitudes, tropics, and SH polar regions are used. The setting for the unperturbed case encompasses the US standard atmosphere water vapour profile, the LOWTRAN (Kneizys et al., 1986) background aerosol profile, an albedo of 0.5, and an effective surface elevation of 4 km. In addition to perturbations of the water vapour profile, the influence of albedo, aerosol, water vapour below the retrieval levels, and effective surface elevation are tested in the simulated retrievals. For these parameters, correction terms are included in the retrieval because they are known to influence the measured intensities.

It must be noted that the retrieval setting for the end-to-end tests differ in one aspect from the setting for real data. Usually, the SNR is estimated from the residuals, but for the

simulated intensities there is no noise. To prevent the retrieval from estimating an unrealistically high SNR, a constant SNR of 500 is assumed. This lies well in the range of the known SNR of 400–700 for the retrieval of real SCIAMACHY data. Different from this, the SNR for the end-to-end test is assumed to be constant and does not decrease with height.

Figure 3 shows the resulting performance of the retrieval for both the standard (unperturbed) profile and perturbed water vapour profiles. To account for the vertical sampling and resolution of SCIAMACHY, all water vapour profiles used as input for the simulation are smoothed with the AVK of SCIAMACHY for the direct comparison with the retrieval result (right panel of Fig. 3). The smoothed profile  $\mathbf{x}_{\text{compS}}$  is computed as follows:

$$\mathbf{x}_{\text{compS}} = \exp(\log(\mathbf{x}_a) + \mathbf{A}(\log(\mathbf{x}_{\text{comp}}) - \log(\mathbf{x}_a))), \quad (1)$$

where  $\mathbf{x}_{\text{comp}}$  is the profile which is compared to the retrieved SCIAMACHY water vapour profile  $x_{\text{SCIA}}(z)$ ,  $\mathbf{x}_a$  is the a priori profile and  $\mathbf{A}$  is the AVK matrix of the SCIAMACHY water vapour retrieval. Percentage differences for each individual pair of profiles are calculated by

$$\delta_i(z) = \frac{x_{\text{SCIA}}(z) - x_{\text{comp}}(z)}{x_{\text{ref}}(z)} \cdot 100.0, \quad (2)$$

where  $\delta_i(z)$  is the percentage difference for an individual pair of profiles at each altitude  $z$ , and  $x_{\text{comp}}(z)$  is the original or smoothed data for comparison. For the end-to-end tests  $x_{\text{ref}}(z)$  is equal to  $x_{\text{comp}}(z)$ , i.e. the profile which was used to calculate the intensities with SCIATRAN.

There is a large difference between the smoothed and non-smoothed result in the cases where the water vapour profile is only perturbed in a narrow layer. Above 22 km height, the smoothing also has a large influence on the result for several other cases. This shows that the given resolution does not allow us to resolve narrow vertical layers and that the water vapour above 22 km is influenced by the profile below due to the vertical resolution, as already discussed in Sect. 2.1. Accounting for the resolution effects, the errors are usually smaller than 5 %.

There is some error even for the unperturbed case. This is mainly caused by the retrieval of the tropospheric contribution parameter. Although the first guess for the effective surface elevation is set to the correct result, it is changed during the retrieval. The implementation of the retrieval for the tropospheric contribution parameter and the fast simplified multiple scattering scheme used in the first three iterations contribute to this error. The effective elevation is the first part of the tropospheric contribution parameter that is estimated during these first iterations with the fast simplified multiple scattering scheme and at least one more iteration. This multiple scattering scheme leads to errors in the effective surface elevation retrieval and hence to errors in the retrieved water vapour profile, also in the unperturbed case. The higher the effective surface elevation is, the larger the errors for the re-

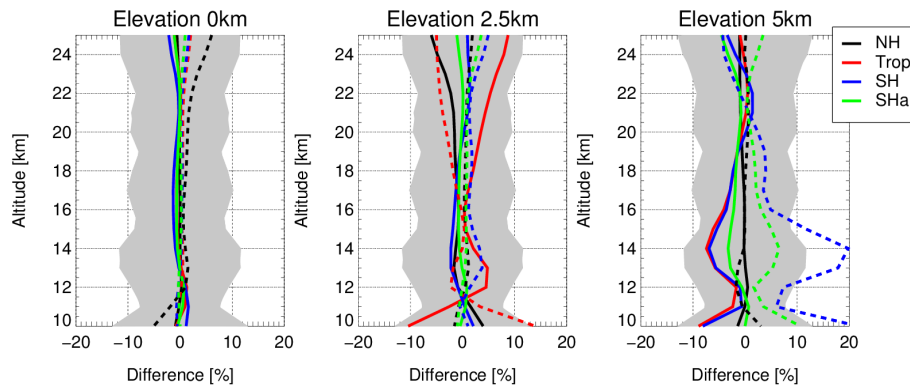


**Figure 4.** End-to-end test for a perturbed albedo and effective elevation. The comparison is done in a similar manner to Fig. 3 for an albedo of 0.1 (solid lines) and 0.7 (dashed lines). The different surface elevations (0, 2.5, and 5 km) are shown in the different panels. The colours mark observation geometries for different regions (NH and SH mid-latitudes, tropics and SH polar regions). The smoothing with the AVK is done for all cases (but has no effect here). The grey shading shows the maximum of retrieval errors.

trieved water vapour profile are. With a reference surface elevation of 4 km as used in our simulation, this error is smaller than 3 % between 10 and 25 km for the unperturbed atmosphere.

The effect from the effective surface elevation can be seen in more detail in Fig. 4, where the results with perturbed albedo and perturbed effective surface elevations are shown. Although the test with 2.5 km elevation and 0.7 albedo (middle panel dashed lines) is closest to the first guess values (4 km and 0.5, respectively), the ones with lower elevation yield smaller errors in the water vapour profile (left panel). This is because a higher elevation and a higher albedo increase the influence of the multiple scattering from below the tangent altitudes on the water vapour retrieval. For an elevation of 0 or 2.5 km all deviations from the true water vapour profile are smaller than 5 % between 11 and 22 km. For an elevation of 5 km there are larger ones; especially if the albedo is 0.7, the deviations even exceed 10 % for some altitudes. For the different observation geometries the sign and vertical structure of the errors vary, but their magnitude is comparable for 0 and 2.5 km elevation. For 5 km elevation the errors are larger for cases with an albedo of 0.7 for some observation geometries. The retrieval for the geometry used in the tests for the tropics yields an error which did not occur in the retrievals for measured data (not shown). For measurements, the retrieval usually results in a low albedo of 0.1 or less (about 65 % of all cases for April 2004). For the elevation there are many cases with low elevations but e.g. about 55 % of all cases for April 2004 have an effective elevation of 3.5–4.5 km. These elevations are related to scenes with thick clouds in the troposphere. Many real scenarios are probably best represented by the test with 5 km elevation and an albedo of 0.1, which leads to errors of up to about 7 % above 11 km.

Prior to the water vapour retrieval, the aerosol profile is retrieved (Roazanov et al., 2011a). Figure 5 shows the difference between the retrieved and the true water vapour, if the aerosol

extinction profile is perturbed compared to the LOWTRAN background profile used as first guess. Here, first the aerosol profile is perturbed and used to calculate the simulated intensities for the aerosol retrieval. With them, a new aerosol profile is retrieved for 12–35 km height. The perturbed profile is also used to simulate the intensities for the water vapour retrieval. This retrieval uses the aerosol profile from the aerosol retrieval. In the end, the water vapour profile is compared to the reference water vapour profile to estimate the effect from a perturbed aerosol profile.

The aerosol profile is perturbed for two different height ranges: the whole profile and only heights up to 30 km. The latter are well covered by the aerosol retrieval. The aerosols show a much larger influence on the retrieved water vapour profile for a perturbation of the whole profile (including heights above the retrieval height) than for a perturbation up to 30 km. The effects on the water vapour profile exceed 50 % at some altitudes and geometries if the whole aerosol profile is multiplied by a factor of 2 or 10. For the tropical geometry a factor of 10 leads to an error, which was not observed for profiles retrieved from measurements (not shown). A perturbation with a factor 10 for the whole aerosol profile is larger than one would expect in nature. If only the heights up to 30 km (where the aerosol retrieval can correct the profile) is perturbed the error on the water vapour profile is smaller than 5 % below 23 km. For smaller perturbations the effect on the water vapour retrieval is smaller, too. The errors are lowest for the NH. Nevertheless, it is important to note, that an unknown aerosol profile above the retrieval heights of the aerosol retrieval (35 km) can influence the result of the water vapour retrieval. Although the aerosol is not well known at these altitudes, it can be expected that the natural variability is smaller there than below (see e.g. Salazar et al., 2013). Recent volcanic eruptions did not reach these heights directly, but aerosols are transported by the Brewer–Dobson circulation (BDC) up to above 30 km; see e.g. Vernier et al. (2011).

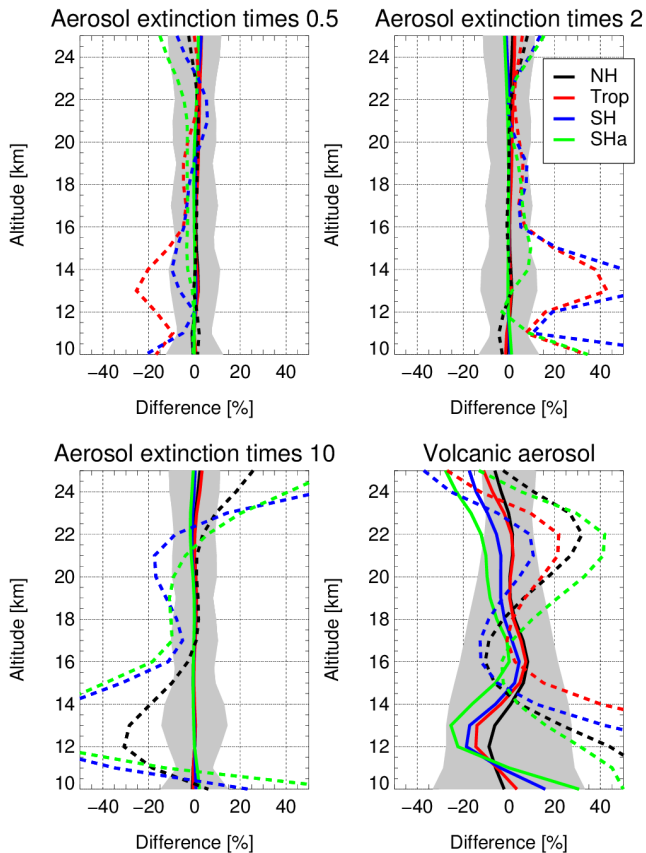


**Figure 5.** End-to-end test for different perturbations of the aerosol profile. In both upper panels and in the lower left panel the dashed lines show cases where the whole aerosol extinction profile (0–100 km) is perturbed by multiplying by a factor (given in the title of each panel); solid lines show cases where the perturbation is limited to 0–30 km. The lower right panel shows cases where the background aerosol profile is exchanged with cases for aged moderate (solid lines) and fresh high (dashed lines) volcanic aerosol according to the LOWTRAN model. The four colours show different observation geometries. The smoothing with the AVK is done for all cases. The grey shading shows the maximum of retrieval errors.

Above 40 km, meteoritic smoke influences the aerosol extinction (e.g. Neely et al., 2011). There is also a known latitudinal gradient in stratospheric aerosol load which is not considered by the a priori aerosol profile used. The perturbations by factors of 0.5 and 2 probably represent a realistic variability, at least up to 30 km but possibly also above.

Because not only the aerosol extinction, but also changes in the aerosol type and size distribution can have an effect on the water vapour retrieval, the LOWTRAN model is used to simulate two different cases with volcanic aerosols. For a moderate amount of aged volcanic aerosols, errors up to about 30 % are found for some heights and observation geometries. It should be noted that although the aerosol extinction is also increased in these cases, the resulting errors in the water vapour profiles have, at some altitudes, the opposite

sign compared to the cases where the extinction is increased by a factor of 10. This shows that the effect of aerosols on the water vapour retrieval cannot be explained by changes in the aerosol extinction alone. For high amounts of fresh volcanic aerosols, the errors in the water vapour profile are even larger, sometimes exceeding 50 %. For measurements, cases with a very high load of volcanic aerosols are usually filtered out by the cloud filter; see Eichmann et al. (2015).

Due to multiple scattering the properties of the atmosphere below the retrieval altitudes can influence the measured radiances, too. To correct for this influence, the tropospheric contribution parameter estimates a scaling factor for the water vapour profile below 10 km. The effect from the perturbations of the water vapour and aerosol profile below 10 km is shown in Fig. 6. The water vapour and aerosol retrieval cannot retrieve the shape of the corresponding profiles there. Perturbing the water vapour with a factor of 10 shows a large error in the lowest part of the profile only, up to about 13 km. Above, the error is comparable to the one caused by the smaller perturbations and is usually smaller than 5 %. A perturbation of the aerosol profile below 10 km can also cause large errors in the retrieved water vapour above about 18 km. The reason is most probably that the tropospheric contribution parameter corrects for changes in the water vapour profile below 10 km but not for the aerosol profile. Additionally, the water vapour absorption lines are likely saturated if the water vapour reaches typical amounts for the lower troposphere. This result indicates that the retrieval result can be influenced by layers with increased aerosol extinction even if they are below 10 km. It should be noted that although tests performed here use perturbations of the whole column starting from the ground, the aerosols at altitudes just below 10 km have a larger effect on the water vapour retrieval than the ones close to the earth surface. Such layers can be formed by strong volcanic eruptions and fires. The water vapour amount below the lowest retrieval level has a large effect on the retrieval result mainly below 13 km.

Altogether, the end-to-end tests show that the water vapour retrieval works well even when the a priori water vapour profile is quite different from the true state. The vertical resolution of the retrieval must be considered, because wet or dry layers that are narrow compared to the resolution cannot be resolved and altitudes above 22 km are not independent of the ones below. Especially the aerosols both below and above the heights of the aerosol retrieval (12–35 km) and high effective surface elevations can cause errors in the retrieved water vapour profile. Usually, these errors are well below 10 % but can be larger for extreme cases (e.g. volcanic eruptions). It should be noted that systematic changes in the aerosol content of the atmosphere can introduce systematic errors in the water vapour profiles. The water vapour column below the retrieval levels can lead to errors in the water vapour profile above, but mainly for the lower part of the profile with errors larger than 10 % observed up to 12 km height.

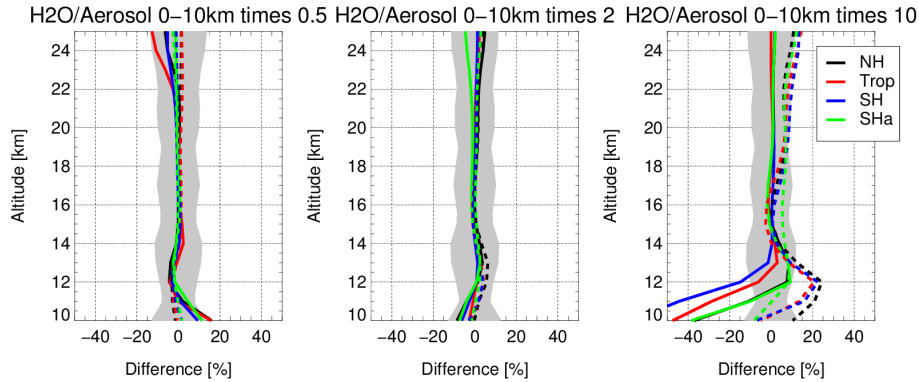


**Figure 6.** End-to-end test for different perturbations of the aerosol (dashed lines) and water vapour (solid lines) profile below the retrieval heights (0–10 km). The four colours show different observation geometries; the three panels show different perturbations. The grey shading shows the maximum of retrieval errors. The smoothing with the AVK is done for all cases.

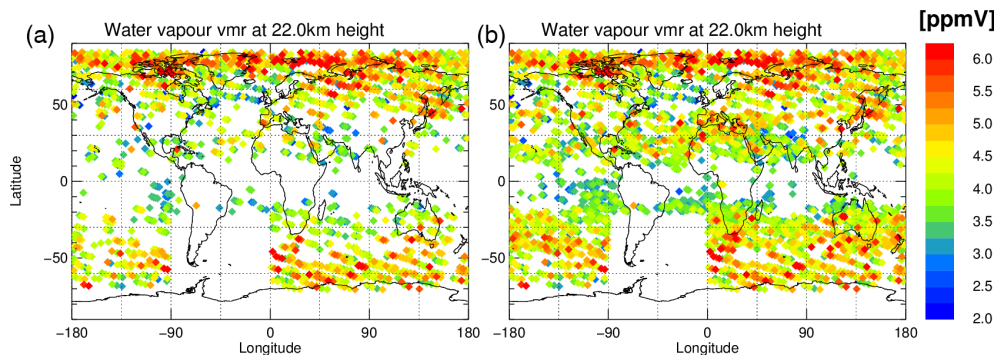


**Figure 7.** Coverage of the water vapour retrieval from SCIAMACHY limb measurements for April 2004. The position of each profile is indicated; the colour scale shows the volume mixing ratio of water vapour at 22 km height. Data are shown for (a) every eighth day globally (1, 9, 17, 25 April) and (b) every eighth day globally and every second day between 45° S and 45° N.

To summarize, the errors expected from the end-to-end tests are smaller than 10% above 12 and below 22 km for usual atmospheric conditions if the resolution of the profile is taken into account. In the lowest and uppermost part of the profile, larger errors are possible.

### 2.3 Cloud filtering and data coverage

Envisat had a sun synchronous orbit with an equator crossing time of 10:00 UTC (Gottwald and Bovensmann, 2011). Due to the inclination of the orbit, measurements took place later than 10:00 UTC in the NH and before 10:00 UTC in the SH. There were 14.4 orbits of Envisat per day and global coverage was reached within about 6 days for SCIAMACHY limb measurements at the equator (Bovensmann et al., 1999). The water vapour retrieval is based on measurements of scattered sunlight, therefore only day side measurements of SCIAMACHY during the descending phase of the orbit can be used. The retrieval is only performed with solar zenith angles smaller than 85°. Since the solar zenith angle changes with season, this leads to a seasonal dependence of coverage. In the summer hemisphere the measurement positions

reach further polewards. The region between about 50° S and 60° N is covered the whole year. This region is not symmetric around the equator, because the equator crossing time is 10:00 UTC (not 12:00 UTC). Therefore, higher latitudes are covered in the NH than in the SH during corresponding seasons. This can for example be seen in Fig. 8d, where the highest latitude covered during winter is usually between 60 and 70° N in the NH and between 50 and 60° S in the SH.

The computation of the water vapour retrieval is very time-consuming despite the usage of high-performance computer clusters like the one from HLRN (Norddeutscher Verbund zur Förderung des Hoch- und Höchstleistungsrechnens, English: North-German Supercomputing Alliance). Using HLRN and the computer infrastructure at IUP Bremen, the retrieval of 1 day of SCIAMACHY data was possible each day. Therefore, in the beginning only every eighth day was calculated to provide a time series from August 2002 to April 2012. Figure 7a shows the water vapour mixing ratios at 22 km height for all measurement positions used in V3.01 for every eighth day in April 2004 (1, 9, 17, and 25 April). Due to higher cloud top heights the data are more sparse in

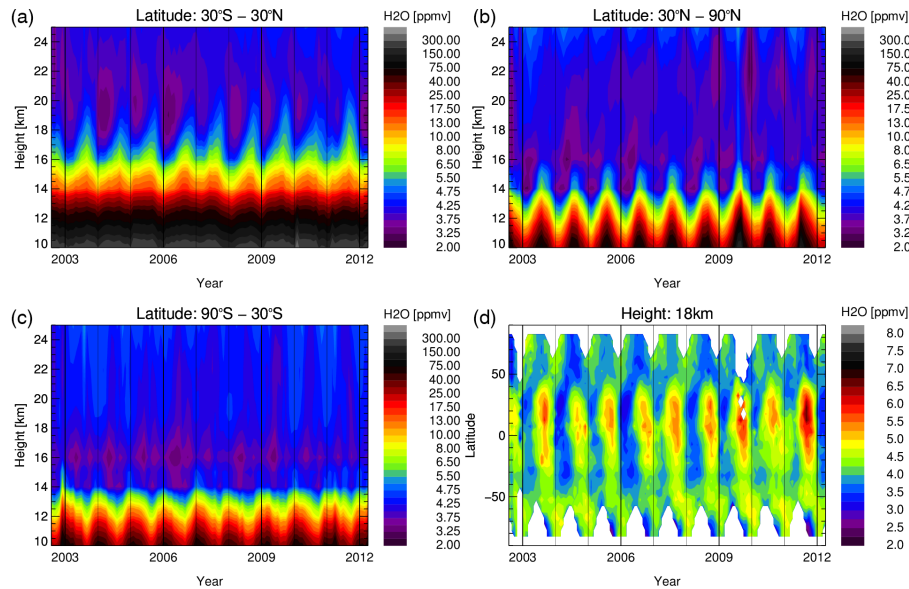


**Figure 8.** Time series of water vapour volume mixing ratios from SCIAMACHY limb measurements three latitude bands: 30–90° N, 30° S–30° N, and 90–30° S and for all latitudes at 18 km height. Area weighted means of  $5^\circ \times 5^\circ$  gridded data.

the tropics. To account for these gaps in the tropics and to get a more uniform global distribution, V3.01 contains data between  $45^\circ$  S and  $45^\circ$  N for every second day in addition to the global data. Figure 7b shows this extended data set for April 2004.

The cloud filter is the same as discussed in Rozanov et al. (2011a). Clouds can be identified in SCIAMACHY measurements with the SCIAMACHY Cloud Detection Algorithm (SCODA), which uses a colour ratio method (see von Savigny et al., 2005a, and Eichmann et al., 2009, 2015). We use V1.9 of the cloud filter with three wavelength pairs – 750, 1090 nm; 1090, 1552 nm; and 1552, 1685 nm – and exclude all profiles where clouds are detected at altitudes higher than 10 km.

Additionally, measurements taken when Envisat was within the South Atlantic Anomaly (SAA) are excluded because electronic noise can perturb the measurements here (Gottwald and Bovensmann, 2011). Therefore, no profiles exist in a region ( $60\text{--}20^\circ$  S,  $90^\circ$  W– $5^\circ$  E) over South America (see Fig. 7). Note that the position of the satellite, not the tangent point of the LOS, is relevant to avoid the SAA.

An additional filter is applied: all profiles where the retrieval does not converge within 12 iterations are omitted. This is slightly different to the water vapour data V3.0 used in SPARC-DI (Stratosphere–troposphere Processes And their Role in Climate – Data Initiative; Hegglin et al., 2013, 2014), where profiles are only omitted if the retrieval does not reach convergence after 12 iterations and the RMS of the residual is larger than 0.01. Additionally, V3.0 has a different data coverage using only every fourth instead of every second day between  $45^\circ$  S and  $45^\circ$  N.

The cloud filter is sensitive to high stratospheric aerosol loadings (Eichmann et al., 2015), as they were observed after the eruptions of Kasatochi and Sarychev (e.g. Di Pierro et al., 2013). This leads to reduced coverage over the NH especially in Autumn 2009. This can be seen in Fig. 8d, where the time series of monthly mean data is shown on a  $5^\circ \times 5^\circ$  grid for 18 km height. Since the end-to-end tests (Sect. 2.2) show an effect of aerosols on the water vapour retrieval, it is favourable that profiles affected by large amounts of aerosols are excluded. Figure 8a–c show the monthly and zonal means of water vapour volume mixing ratios for three latitude bands (30–90° N, 90–30° S, and 30° S–30° N) between 10 and 25 km. The zonal bands are averaged from  $5^\circ \times 5^\circ$  gridded data and an area weighted mean is applied. As described before, not all available measurements are used, but the monthly means are based on every second day between  $45^\circ$  S and  $45^\circ$  N and every eighth day polewards of this region.

### Time series analysis

To analyse the data set further we used a multivariate linear regression similar to the one presented in Gebhardt et al. (2014) for zonal monthly mean water vapour volume mixing ratios on a  $5^\circ$  latitude grid. The fit parameters are constant term, linear change, 12- and 6-month sine and cosine terms, as QBO (quasi-biennial oscillation) proxies the 10 and 30 hPa Singapore winds (Naujokat et al., 1986, from <http://www.geo.fu-berlin.de/en/met/ag/strat/produkte/qbo/>), and the Mg II Index as solar cycle proxy. The Mg II Index is based on GOME, SCIAMACHY, and GOME II data (Snow et al., 2014; Weber et al., 2013)

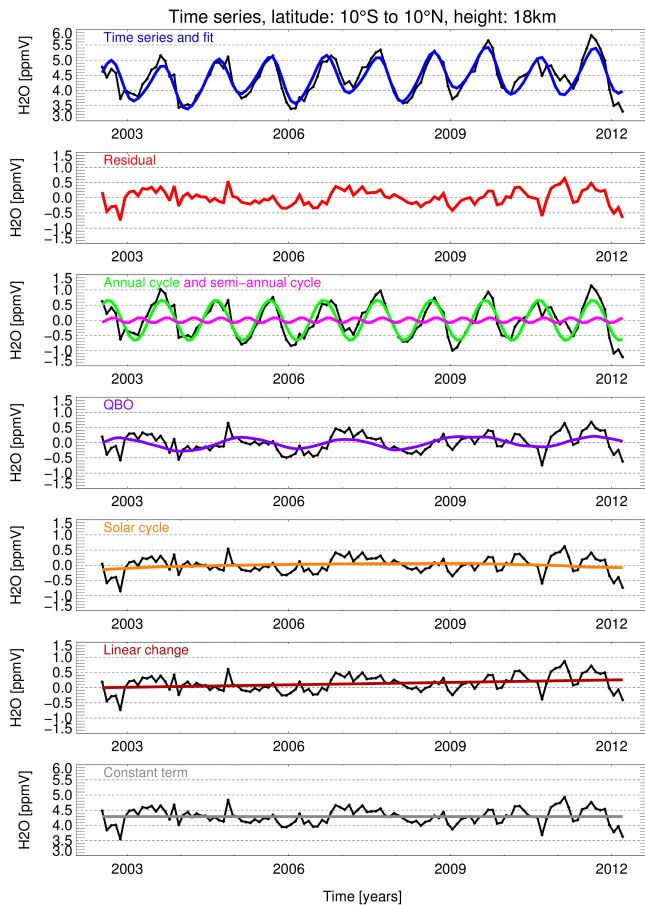


**Figure 9.** Monthly mean zonal mean water vapour volume mixing ratio time series from SCIAMACHY for  $10^{\circ}\text{S}$ – $10^{\circ}\text{N}$  and 18 km height. The black line in the top panel shows the SCIAMACHY time series. The coloured lines in the lower panels show the different fit parameter terms, the red line in the second panel the residual. In the lower panels the black curves show the fit parameter terms shown in the corresponding panel plus the residual shown in the second panel.

and is available at [http://www.iup.uni-bremen.de/gome/solar/MgII\\_composite.dat](http://www.iup.uni-bremen.de/gome/solar/MgII_composite.dat). As an example, Fig. 9 shows the time series, the different fit parameters, and the residual for 18 km altitude and  $10^{\circ}\text{S}$ – $10^{\circ}\text{N}$ .

Figure 10 shows the resulting linear trend in percent per decade. Non-significant trends are marked with crosses. The criteria for significance is that the trend is larger than the  $2\sigma$  error of the linear term. The error of the fits are calculated based on the fit residuals. There are significant positive trends in the tropical and subtropical lower stratosphere as well as at about  $50$ – $60^{\circ}\text{S}$  and in the northern mid-latitudes and high latitudes up to about 16 km. In the inner tropics ( $10^{\circ}\text{S}$  and  $10^{\circ}\text{N}$ ) the water vapour increases with about 10 % per decade above 20 km from August 2002 to April 2012. The linear change in the NH in the mid-latitudes and high latitudes up to about 16 km reaches very high values at

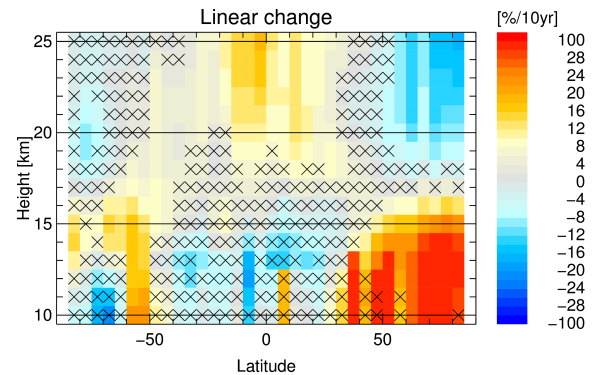


**Figure 10.** Linear change from the multivariate linear regression for SCIAMACHY zonal mean data on a  $5^{\circ}$  latitude and 1 km height grid. Non-significant values ( $< 2\sigma$ ) are marked with crosses.

some places larger than 30 % per decade. Significant negative trends of about 6–16 % per decade are found in the NH and SH high-latitude stratosphere above 18–19 km.

Figure 11 shows the amplitude and the phase of the annual cycle. The amplitude is shown as percentage value of the mean water vapour at each altitude and latitude bin, the phase is shown as month of the year, in which the annual cycle has its maximum. One can see that in relation to the mean water vapour the annual cycle is largest in the troposphere in both the subtropics and mid-latitudes. Up to about 10 km at  $65^{\circ}\text{N}$  and 15 km at  $25^{\circ}\text{N}$  and up to 12 km between  $50$  and  $30^{\circ}\text{S}$ , the amplitudes are larger than the mean value. Larger amplitudes are observed in the NH than in the SH. There are also large percentage amplitudes in the SH high latitudes, both in the troposphere and stratosphere. The annual cycle has its highest amplitude in the summer hemisphere below about 15 km. In the inner tropics ( $10^{\circ}\text{S}$ – $10^{\circ}\text{N}$ ) the maximum is found in spring and early NH summer below about 14 km. Above, one can see the tape recorder effect (e.g. Mote et al., 1996), i.e. the month of the maximum changes from July to October with increasing height, up to about 19 km altitude. Above, the tape recorder is not visible and the month of the maximum changes back to June and May in the inner tropics. In these months the maximum is also found in the NH stratosphere above about 22 km. In the extratropical SH stratosphere the maximum above 22 km is found in December to January. Between 15 and 20 km the maximum is usually in January to March in the NH and SH polewards of about  $60^{\circ}$  latitude. Equatorwards of about  $50^{\circ}$  latitude it is found in August and September in the NH and mainly in October in the SH.

### 3 Comparisons

Within SPARC-DI SCIAMACHY limb water vapour V3.0 was compared to several other satellite data sets (Hegglin et al., 2013). V3.01 differs only in two aspects from V3.0:

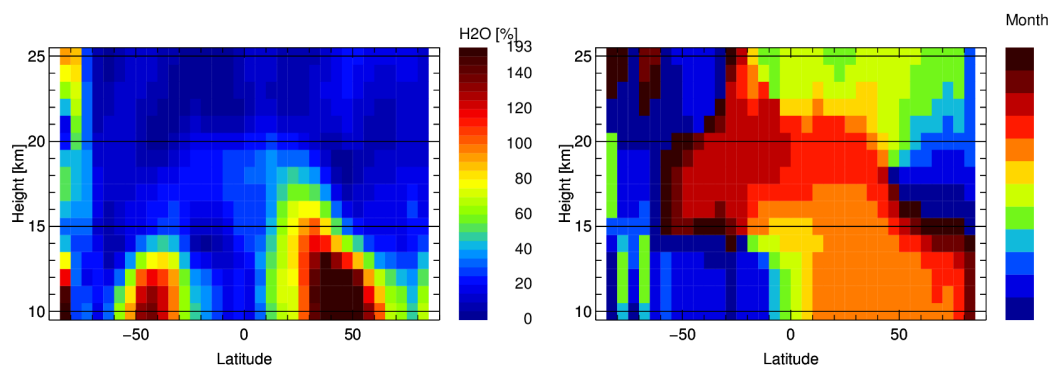


**Figure 11.** Amplitude and month of the maximum (1: January, 12: December) for the annual cycle from the multivariate linear regression applied to SCIAMACHY data on a  $5^\circ$  latitude and 1 km height grid.

more data are processed here, leading to a denser sampling (every second instead of every fourth day between  $45^\circ$  S and  $45^\circ$  N) and a stricter filter for convergence is applied (all non-converging retrieval are excluded, for V3.0 only the ones which exceed a threshold on the RMS of the residual). In Khosrawi et al. (2015) V3.01 was used. There are only small changes between V3.0 and V3.01 data as shown within the SPIN (ESA SPARC Initiative) project (Van Roozendaal et al., 2015). Nevertheless, a comparison to in situ and satellite data is presented here to provide an overview of the quality of the SCIAMACHY data set. In contrast to SPARC-DI where zonal mean data were compared we focus on comparisons of collocated profiles, the stability of observed differences over the complete measurement period of SCIAMACHY, differences found from the time series, and the effect of the vertical resolution of the SCIAMACHY profiles on the comparison.

Balloon measurements using a frost point hygrometer (FPH) are used for comparison with the SCIAMACHY data. The balloon launches took place in Boulder, Colorado, Hilo, Hawaii and Lauder, New Zealand; see Hurst et al. (2011) for a description of the FPH data. The averaged profile from both ascent and descent is used. This is a different set of data than the one used in Rozanov et al. (2011a); it covers newer measurements, different stations, and only profiles included in the temporal sampling of V3.01.

The Fast In situ Stratospheric Hygrometer (FISH; Zoeger et al., 1999; Kunz et al., 2014; Meyer et al., 2015) measures the total water and can be carried by various airborne platforms. Here, we only use data when the FISH was on-board the high-altitude research aircraft M55-Geophysica to get profiles up to about 20 km. Data are not available on a regular basis but during several measurement campaigns (Schiller et al., 2008). For the following campaigns we found collocations to SCIAMACHY measurements: TROCCINOX (Tropical Convection, Cirrus, and Nitrogen Oxides Experiment, e.g. Konopka et al., 2007) in 2005, the CRISTA-NF (Cryogenic Infrared Spectrometers and Telescopes for the Atmosphere – New Frontiers) test flights and SCOUT-O3

(Stratosphere-Climate links with emphasis On the UTLS- $O_3$ ; Cairo et al., 2010) in 2005, AMMA (African Monsoon Multidisciplinary Analyses, Redelsperger et al., 2006) in 2006, and RECONCILE (Reconciliation of essential process parameters for an enhanced predictability of Arctic stratospheric ozone loss and its climate interactions, von Hobe et al., 2013) in 2010. To compare the FISH total water measurements (gas-phase water and ice crystals) with the water vapour profiles retrieved from SCIAMACHY measurements only FISH measurements for subsaturated conditions are used in order to omit cirrus clouds. To extract profiles from the FISH measurements, data during the descent of single M55-Geophysica flights are used. As descent, we define the part of the flight after the last time the plane was less than 200 m lower than the maximum flight altitude. This definition was chosen to omit long flight lags with approximately constant height. The position and time of the last valid measurements during the flight are used as time and position of the profile. Ascending profiles are not used to omit data with possible contamination from wetter air from lower altitudes.

Water vapour profile retrievals are possible from different observation geometries of SCIAMACHY. In addition to limb measurements, lunar and solar occultation measurements are available from SCIAMACHY (e.g. Noël et al., 2009). For the SCIAMACHY occultation measurements, the SNR is much higher but the sampling is lower than for limb measurements. For each orbit, there is only one solar occultation measurement in the NH and a maximum of one lunar occultation measurement in the SH. The availability of lunar occultation also depends on the moon phase. The water vapour retrieval from lunar occultation measurements is presented in Azam et al. (2012); the solar occultation algorithm is similar to the one used for lunar occultation. Different from the data set in Azam et al. (2012), the lunar occultation data version used here includes ECMWF analysis pressure and temperature fields instead of the US standard atmosphere model. Both types of occultation measurements have a distinct seasonal cycle in the measurement latitudes, which makes the analysis of the time series challenging. However they are

well suited for comparisons to collocated limb water vapour profiles because occultation retrievals usually have a better data quality due to the stronger signal and no influence of multiple scattering. It is also advantageous that these measurements are performed by the same instrument (although with different settings) and cover the same time period. However, there is always a temporal and spatial difference between limb and occultation measurements. Especially for the lunar occultation measurements, only a few collocations to the limb measurements are found, because their quality is sufficient only at night time and for a part of the moon phases.

On Envisat, water vapour was also measured by the Michelson Interferometer for Passive Atmospheric Sounding (MIPAS) (e.g. Fischer et al., 2008; Milz et al., 2009; von Clarmann et al., 2009; Stiller et al., 2012). Because the platform is the same for MIPAS as for SCIAMACHY, there is only a small time difference between the measurements with similar tangent point positions (about 25 min). While SCIAMACHY looks forward for limb measurements, MIPAS looks backward. Additionally, the angle between the satellite track and the LOS is different for MIPAS and SCIAMACHY, because SCIAMACHY looks further off track to adjust to the nadir measurement positions and to measure several adjacent limb profiles. The tangent point position difference between MIPAS and SCIAMACHY is largest in the mid-latitudes, leading to fewer collocations in this area. MIPAS measures the atmospheric emission in the mid-infrared spectral range (Fischer et al., 2008). Here, we use the reduced resolution data starting in January 2005, data version V5R. The data are filtered to omit profiles with visibility flag equal 0 (indicating clouds) and diagonal elements of the AVK smaller than 0.03, as described by e.g. Lossow et al. (2011). We excluded all profiles with these values between 10 and 25 km height.

ACE-FTS (Atmospheric Chemistry Experiment – Fourier Transform Spectrometer) on SCISAT is a solar occultation instrument measuring in the mid-infrared spectral range (e.g. Bernath et al., 2005; Carleer et al., 2008; Hegglin et al., 2013). ACE-FTS measurements are available from 2004 onwards. Here, version 3.0 (Boone et al., 2013; Waymark et al., 2013) is used. The time period used stops in September 2010, which is recommended for this data version. ACE-FTS data are filtered to exclude profiles where relative errors larger or equal to 1 occur between 10 and 25 km height.

Another solar occultation instrument is the Halogen Occultation Experiment (HALOE) (Russell et al., 1993). Here, data version 19 (v19) is used, which is the third public release of the HALOE data (Grooß and Russell, 2005). The HALOE water vapour retrieval is described in Russell and Swider (1991) and Remsberg et al. (1990) and data are available between October 1991 and November 2005.

The Microwave Limb Sounder (MLS) is an instrument on the Aura satellite, which has measured thermal microwave emission in the limb viewing geometry since August 2004

(Schoeberl et al., 2006). The water vapour retrieval is described in Read et al. (2007). Version 3.3 (v3.3) data used here were validated by Hurst et al. (2014). We use interpolated ECMWF geopotential heights instead of the geopotential heights provided by MLS to convert from pressure to geometric altitudes. The MLS data are screened only to use profiles whose status flag is zero and a precision greater than 0 for water vapour, temperature, and geopotential height. In addition to the previous checks, for water vapour only profiles, we apply an additional requirement that its quality is greater than or equal to 1.3 and has a convergence less than 2. Sometimes good profiles still have erroneous values and we reject instances where water vapour values are less than 0.1 ppmv for pressures between 178 and 0.019 hPa and less than 1.0 ppmv for levels with pressures greater than 178 hPa. For temperature and geopotential heights the threshold values are 1.2 for convergence and 0.65 for quality.

SAGE (Stratospheric Aerosol and Gas Experiment) II was a solar occultation instrument on the Earth Radiation Budget Satellite (ERBS) (Mauldin et al., 1985). SAGE II operated between October 1984 and August 2005; here we use the most recent data version 7 (v7.0) (Damadeo et al., 2013).

### 3.1 Methods

To compare SCIAMACHY water vapour retrieval results to other data sets, only collocated profiles are used. The collocation criteria are listed in Table 1 and differ for the various data sets. For comparisons to other limb satellite measurements with a dense horizontal coverage more strict collocation criteria are used than for occultation and in situ measurements, which are usually more sparse. The comparisons are performed in number densities as this is the quantity directly retrieved from SCIAMACHY measurements. All comparison data sets given in volume mixing ratio provide simultaneously measured temperature and pressure data which allow the consistent conversion to number densities. Collocations are not used if the modified potential vorticity, which is calculated for the position of each profile from ECMWF Interim wind data, differs by 3 PVU or more to omit the comparison of profiles inside and outside the polar vortex.

Usually, only smoothing with the AVKs is performed when high resolution data are compared with remote sensed data with a much lower resolution. Theoretically, the smoothed data set should have infinitely dense data (von Clarmann, 2006). When comparing different satellite data sets, the smoothing with the AVKs is often omitted, assuming that the agreement is sufficiently high between the resolutions of the data sets (e.g. Dupuy et al., 2009; Milz et al., 2009). von Clarmann (2006) proposed to smooth the data with each others' AVK and vice versa.

Only the in situ measurements have much higher vertical resolution than the SCIAMACHY data, so that smoothing using the AVK is obviously needed. We decided to smooth all data sets with the SCIAMACHY AVK following Eq. (1)

**Table 1.** Collocation criteria and number of collocations for the data sets used for comparison with SCIAMACHY limb measurements.

| Instrument and data version | Time difference (h) | Distance (km) | Period used | Number of collocations |
|-----------------------------|---------------------|---------------|-------------|------------------------|
| Balloon FPH                 | 6                   | 1000          | 2005–2012   | 126                    |
| ACE-FTS V3.0                | 6                   | 500           | 2004–2010   | 1602                   |
| FISH on M55-Geophysica      | 12                  | 1000          | 2005–2010   | 42                     |
| HALOE V19                   | 6                   | 500           | 2002–2005   | 1348                   |
| MIPAS V5R                   | 6                   | 200           | 2005–2012   | 26 082                 |
| MLS V3.3                    | 6                   | 100           | 2004–2012   | 13 680                 |
| SAGE II V7.0                | 6                   | 500           | 2005–2005   | 1297                   |
| SCIAMACHY solar occultation | 12                  | 500           | 2002–2012   | 4949                   |
| SCIAMACHY lunar occultation | 12                  | 500           | 2004–2012   | 258                    |

for the following reasons. Several other satellite data sets, e.g. from ACE-FTS have a slightly higher vertical resolution than SCIAMACHY; the data sets with a vertical resolution similar to SCIAMACHY (e.g. MIPAS and MLS) have a different, usually denser vertical sampling than SCIAMACHY. For the in situ data, both interpolated and smoothed data are displayed to provide indications as to which differences are caused by the sampling and resolution of SCIAMACHY. The AVKs of the other satellite data are not used because they are not always available.

For the comparison of the individual profiles we use Eq. (2), where  $x_{\text{comp}}(z)$  is the data for the comparison, which is either interpolated on the SCIAMACHY retrieval grid or smoothed with the SCIAMACHY AVK. Here, for all data sets the reference  $x_{\text{ref}}(z)$  is calculated as

$$x_{\text{ref}}(z) = (x_{\text{SCIA}}(z) + x_{\text{comp}}(z)) \cdot 0.5. \quad (3)$$

Similar to other validation studies (e.g. Dupuy et al., 2009, and references therein) we calculate the percentage difference ( $\Delta(z)$ ), the standard deviation of the bias-corrected difference, and the standard error of the mean (SEM( $z$ )) given by

$$\Delta(z) = \frac{1}{N(z)} \sum_{i=1}^{N(z)} \delta_i(z), \quad (4)$$

$$\sigma(z) = \sqrt{\frac{1}{N(z)-1} \sum_{i=1}^{N(z)} (\delta_i(z) - \Delta(z))^2}, \quad (5)$$

and

$$\text{SEM}(z) = \frac{\sigma(z)}{\sqrt{N(z)}}. \quad (6)$$

In this,  $\delta_i(z)$  is the percentage difference for an individual pair of profiles (see Eq. 2) and  $N$  is the number of collocations for each altitude  $z$ .

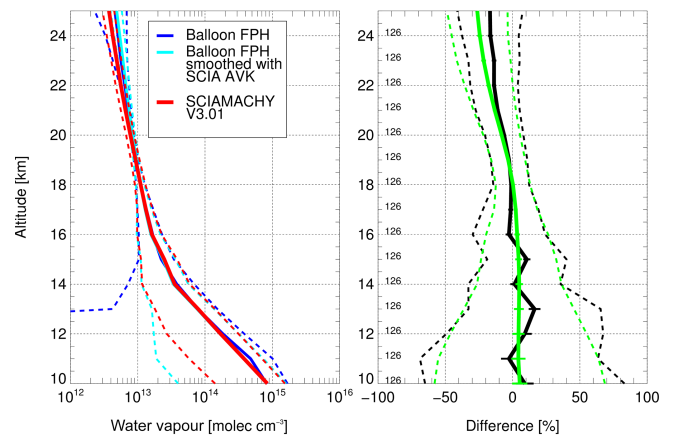


**Figure 12.** Left panel: mean profiles over all collocations from SCIAMACHY and balloon born data (the two lines show the data interpolated on the retrieval grid of SCIAMACHY and smoothed with the AVK of SCIAMACHY, respectively) and their standard deviations (dashed line). Right panel: mean percentage difference between SCIAMACHY water vapour profiles and balloon borne profiles interpolated to the SCIAMACHY retrieval grid (black line) and smoothed with the AVK of SCIAMACHY (green line). The dotted lines show the standard deviation, the error bars (if visible) depict the standard error of the mean. The number of collocations is given for each altitude.

## 3.2 Comparison to in situ data

### 3.2.1 Comparison to balloon data

The left panel of Fig. 12 shows the mean profiles of all collocated balloon and SCIAMACHY observations. For the balloon data, both profiles interpolated to the SCIAMACHY retrieval grid and profiles smoothed with the SCIAMACHY AVKs are shown. Dotted lines mark the mean plus and minus the standard deviation (Eq. 5). The mean percentage difference (Eq. 4) is shown in the right panel of Fig. 12 together with its standard error of the mean (Eq. 6) as error bars and its standard deviation (dashed lines). The SCIAMACHY water vapour profiles agree well with the balloon data smoothed

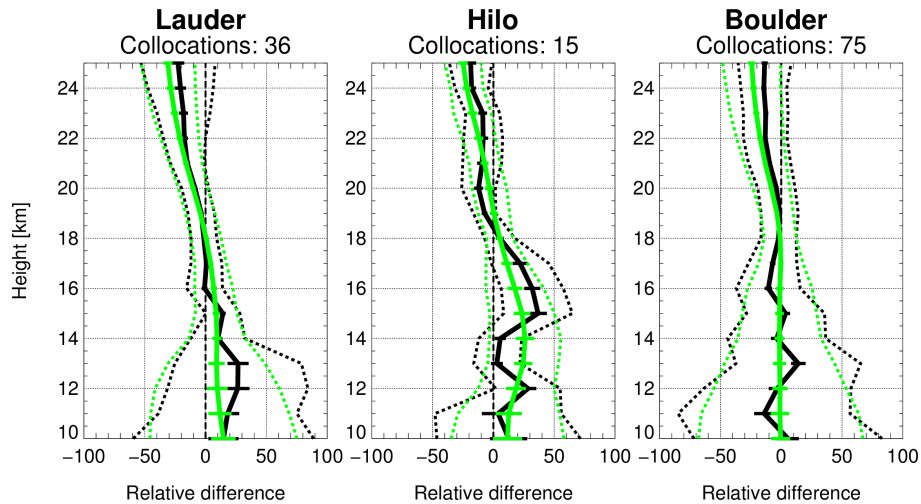


**Figure 13.** Same as right panel of Fig. 12, but for individual balloon stations. Left panel: Lauder (SH mid-latitudes), middle panel: Hilo (tropics), right panel: Boulder (NH mid-latitudes).

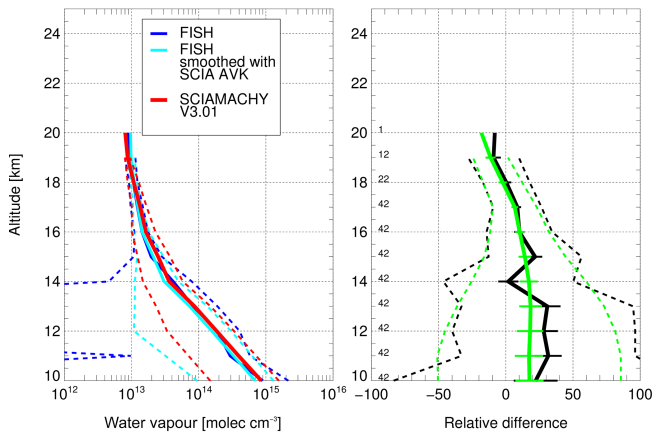


**Figure 14.** Left panel: mean profiles over all collocations from SCIAMACHY and FISH data (the two lines show the data interpolated on the retrieval grid of SCIAMACHY and smoothed with the AVK of SCIAMACHY, respectively) and their standard deviations (dashed line). Right panel: mean percentage difference between SCIAMACHY water vapour profiles and FISH profiles interpolated to the SCIAMACHY retrieval grid (black line) and smoothed with the AVK of SCIAMACHY (green line). The dotted lines show the standard deviation, the error bars (if visible) depict the standard error of the mean. The number of collocations is given for each altitude.

with the AVK. The mean percentage difference is lower than 10 % for most altitudes and lower than 20 % everywhere below 22 km. Both panels of Fig. 12 show that the balloon profiles degraded with the SCIAMACHY AVK agree better with the SCIAMACHY profiles near the tropopause. For the non-smoothed balloon profiles, the shape of the profile is different, especially at about 13 and 15 km height, i.e. at altitudes in between SCIAMACHY measurement heights. This em-

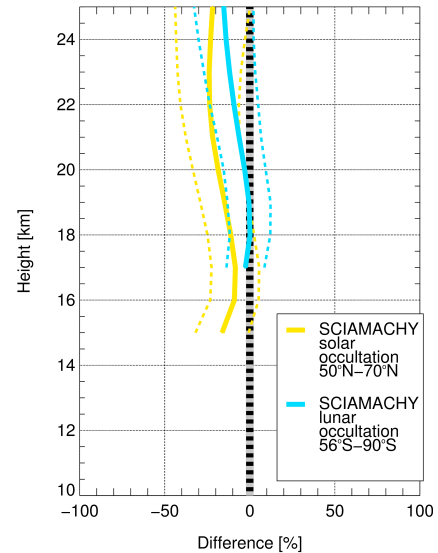


**Figure 15.** Comparison between occultation (lunar and solar) and limb (V3.01) water vapour profiles from SCIAMACHY. The SEM is not visible because it is smaller than the line width.

phasizes that it is important to take the vertical resolution of the retrieved water vapour profiles from SCIAMACHY into account.

Figure 13 shows the mean percentage differences for launches from different balloon stations. Due to the location of these stations (Boulder: 40° N, 105° W; Hilo 19.7° N, 155.1° W; Lauder 45.0° S, 169.7° E) the collocations to the balloon measurement are found in a part of the latitude bands which are used for the satellite comparisons later, i.e. between 60 and 30° S for Lauder, 30° S and 30° N for Hilo, and 30 and 60° N for Boulder. As in Fig. 12 there are differences between the interpolated balloon profiles and the ones

smoothed with the SCIAMACHY AVK. These differences exist for all stations and are largest for Hilo (i.e. in the tropics).

The reason is most probably that in the mid-latitudes, the shape of the a priori water vapour profile is more similar to the shape of the expected real profile. For all stations, SCIAMACHY water vapour V3.01 is drier above about 20 km with up to 20–30 % difference in maximum. For Boulder the agreement with the balloon data below 19 km is very good, since differences are smaller than the SEM and therefore insignificant. For Lauder (SH mid-latitudes) and Hilo (tropics) there are significant differences below 18 km, where SCIAMACHY water vapour V3.01 is about 10 % (SH) and 10–30 % (tropics) wetter.

### 3.2.2 Comparison to FISH on Geophysica

The comparison to the FISH data is shown in Fig. 14 as the mean of all available profiles. There are no FISH measurements on M55-Geophysica available for the upper part of the profile. Below 16 km the SCIAMACHY water vapour is about 10–20 % higher than the FISH measurement smoothed with the SCIAMACHY AVKs. Between 16 and 18 km the agreement ranges from +10 % at 16 km to –10 % at 19 km. The best agreement between both data sets is found at 18 km altitude. The differences are significant at all altitudes except for 18 km although the SEM is large due to the low number of collocations. The standard deviation is comparable to that for the balloon data in Fig. 12.

### 3.3 Comparison to satellite data

#### 3.3.1 Profiles

Figure 15 shows the mean percentage difference profiles between V3.01 limb measurements and the lunar and solar occultation water vapour from SCIAMACHY. The lower limit of the profiles is set by the occultation data and it must be noted that the location of the collocations differs between the data sets. The lunar occultation water vapour is only available from 17 km upwards and in the SH southwards of about 56° S. Solar occultation profiles start at 15 km and are limited to between about 50 and 70° N. The limb water vapour V3.01 agrees well with lunar occultation data. Up to about 22 km, the mean difference is smaller than 10 %. The difference to the solar occultation data is about 10 % up to 18 km increasing to about 30 % for the highest altitudes.

Figure 16 shows the comparison with collocated profiles from the other satellite instruments averaged over different latitude bands. All comparison data sets are smoothed with SCIAMACHY AVKs. It should be noted, that due to the differing collocation criteria (Table 1), a direct comparison between the instruments used for the SCIAMACHY comparisons is difficult. Because the characteristics of the observed differences depend on the height, we discuss them for three

different height ranges: the upper part of the profile above 19 km, the middle part between about 14 and 19 km, and the lower part below 14 km.

For most latitude bands the SCIAMACHY limb water vapour V3.01 is drier in the upper part of the profile compared to the other data sets. This difference is largest in the NH high latitudes (about 10–30 %) and smallest in the tropics (about 0–10 %).

In the middle part of the profile (about 14–19 km) SCIAMACHY data agree well with most data sets. The agreement is best in the NH mid-latitudes and in the SH outside the tropics. In the NH high latitudes SCIAMACHY water vapour V3.01 is drier compared to most data sets down to about 16 km. In the tropics, the SCIAMACHY limb water vapour is wet compared to several other instruments and agrees best to ACE-FTS and MIPAS in the middle part of the profile.

In the lower, mainly tropospheric part of the profile the spread of differences to the various data sets and the standard deviation for each difference profile are comparably large in all latitude bands. However, the SCIAMACHY profiles are mostly wetter than the other data sets. In the lower part of the profiles the best agreement is again found with ACE-FTS and MIPAS; usually the difference is smaller than 10 % in the SH high latitudes and in the NH. In the NH high latitudes, the agreement to SAGE II is comparably good. In the tropics and the SH mid-latitudes, SCIAMACHY data are more than 20 % wetter than all other instruments below 12 km. MLS and HALOE are drier compared to SCIAMACHY for the lower part of the profile for all latitude bands with up to 50 % (MLS) and up more than 100 % (HALOE).

#### 3.3.2 Time series

Figures 17–19 show the comparisons for 30-day running mean time series from collocated data for selected altitudes. The mean is calculated with Eq. (4) for all collocations in every 30-day time slice. Data points are only shown when two or more collocations are found within 30 days. They indicate, how the comparisons change with time, e.g. if there is a drift or a seasonal cycle in the differences. In the NH high latitudes (Fig. 17, left panel) the absolute value of the difference already seen in Fig. 16 increases with time for 18 and 22 km altitude.

This is similar for the NH mid-latitudes (Fig. 17, right panel). Additionally, here a concordant annual cycle is found in the differences between SCIAMACHY and the other instruments which is not seen as distinctly in the polar regions. For 12 and 15 km the differences to the other instruments vary more. In the mid-latitudes a similar amplitude of the annual cycle can be seen in the difference to MIPAS and MLS, although the average difference is usually small for MIPAS and large for MLS at 12 km. This indicates that the SCIAMACHY time series has a different amplitude of the annual cycle compared to MIPAS and MLS in the mid-latitudes.

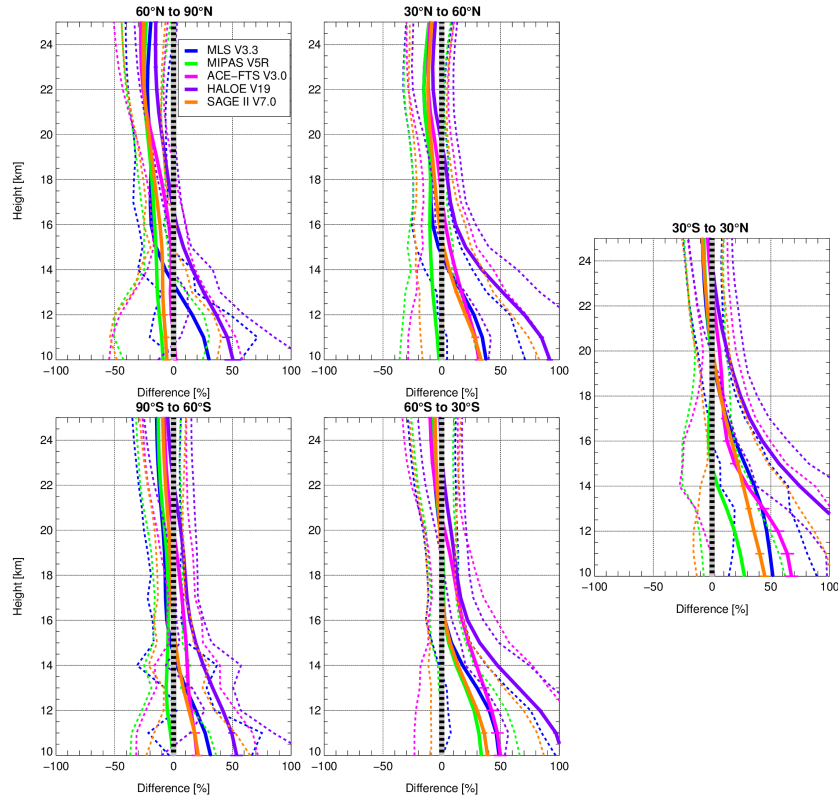


**Figure 16.** Mean percentage difference between SCIAMACHY and other satellite water vapour profiles smoothed with the AVK of SCIAMACHY in each panel. The dotted lines show the standard deviation, the error bars (if visible) of the SEM. The panels show different latitude bands (60–90°, 30–60° N, 30° S–30° N, 60–30°, and 90–60° S).

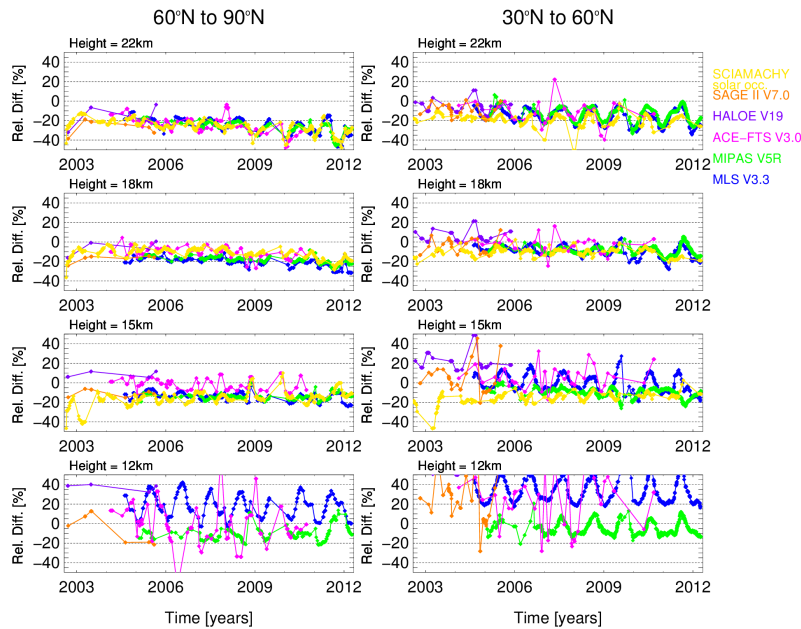


**Figure 17.** 30-day running mean time series of the mean percentage difference between SCIAMACHY and other satellite water vapour profiles smoothed with the AVK of SCIAMACHY (Eq. 4) for different altitudes for polar (left panels) and middle latitude regions (right panels) in the NH.

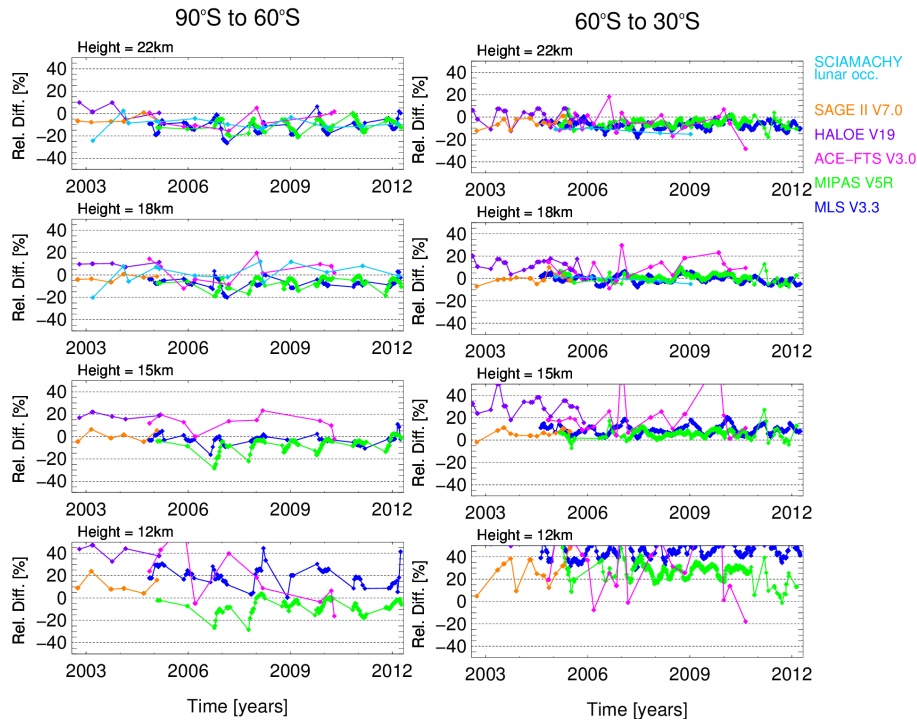


**Figure 18.** Like Fig. 17 for polar (left panels) and middle latitude regions (right panels) in the SH.

For the SH (Fig. 18), there are no obvious drifts in the differences. In the SH, high-latitude differences in the annual cycle are difficult to estimate because SCIAMACHY water vapour is not available during the polar night. There is some annual cycle in the differences in the SH mid-latitudes, but not as clear as in the NH. In the tropics (Fig. 19) there is an annual cycle in the differences to MIPAS at all altitudes, but it is only similar to MLS at 18 and 22 km height. The difference to MLS increases with time at lower altitudes, especially at 12 km, but this is not the case for the difference to MIPAS. There are often too few collocations to see a clear pattern in the differences with the occultation measurements (both from SCIAMACHY and other satellites).

### 3.3.3 Trend and annual cycle

To get a better insight into differences in linear trends and annual cycles, the same linear regression as presented in Sect. 3.3.2 is also applied to the collocated SCIAMACHY and MLS data. This comparison is done for MLS data, because of their dense coverage and the long time overlap with SCIAMACHY. The time overlap with the MIPAS data set used is shorter, because it contains only data from the reduced resolution phase starting in 2005. Using collocated data allows us to analyse the influence of smoothing with the SCIAMACHY AVKs on the multivariate linear regression. In order to use a 5° latitude grid like in Fig. 10, it was necessary to increase the number of collocated data by relaxing the collocation criteria between MLS and SCIA-

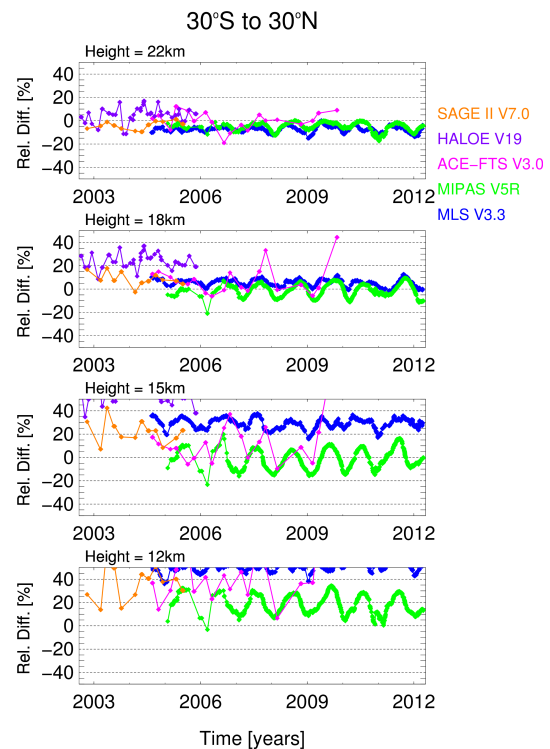


**Figure 19.** Like Fig. 17 for the tropics (30° S–30° N).

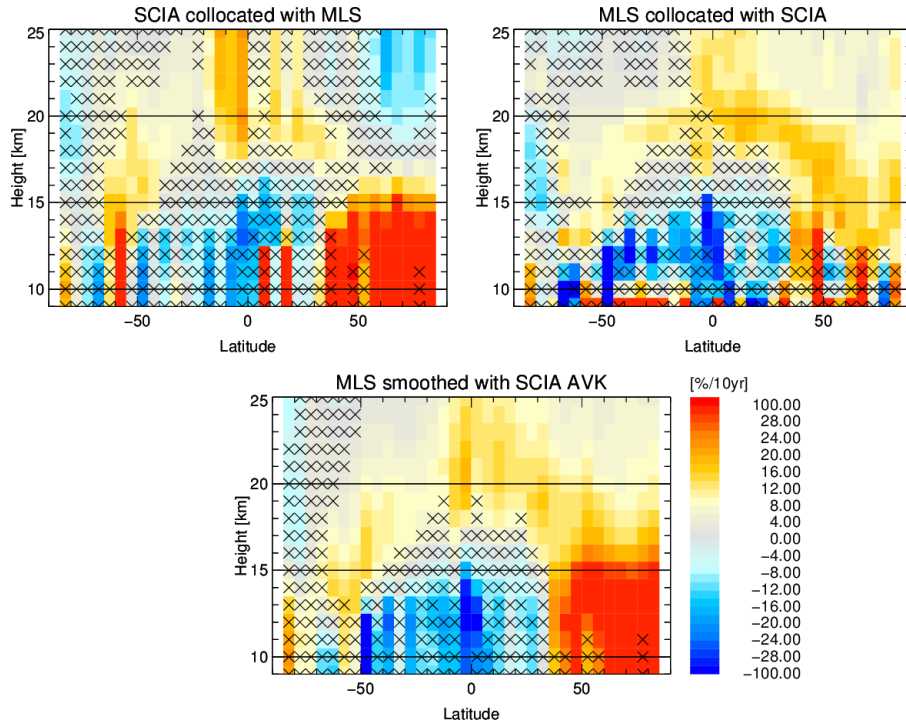


**Figure 20.** Linear trend for zonal monthly mean collocated data from SCIAMACHY and MLS (unsmoothed and smoothed with SCIAMACHY AVKs). Collocations are found between August 2004 and March 2012.

MACHY compared to Table 1 to a time difference of 12 h and a distance of 500 km. Still, there are fewer data points available than in Fig. 10. Collocations are only available for the time period where measurements are available for both instruments (August 2004–March 2012), which shortens the time series. The results for the linear trends can be seen in Fig. 20. The first panel shows the result for SCIAMACHY, the second for MLS, and the third for MLS smoothed with the AVK of SCIAMACHY. Both MLS and SCIAMACHY use sun synchronous orbits and are densely sampled. Therefore, the subsample of collocated profiles should not cause sampling-related drifts, as shown in e.g. the SAGE II data by Damadeo et al. (2014). In the case of SCIAMACHY this is emphasized by the similarity of the SCIAMACHY data collocated with MLS to those for the complete data set shown in Fig. 10 for most latitude bands. Small differences in the magnitude or significance of the trend are probably a result of the reduced length of the time series in Fig. 20. However, there could be differences due to the systematic, latitude-dependent time difference between the SCIAMACHY and MLS measurements. Independent of the subsampling, SCIAMACHY and MLS measurements are taken at systematical different local times.

For collocated MLS, data trends agree well everywhere except in the NH mid-latitudes and the Arctic. Both instruments show significant positive trends in the tropical and subtropical stratosphere and rather negative trends near

the tropopause and SH polar stratosphere. In the NH extratropical stratosphere, MLS shows positive trends, while SCIAMACHY shows negative trends above about 18 km in the high latitudes. The MLS trends near the extratropical tropopause in the NH are mainly positive but not as large as the ones observed by SCIAMACHY. Smoothing the MLS data with the AVK of SCIAMACHY does have some but no large influence on the resulting trends in most areas. Only for the positive trends in the NH high-latitude tropopause region the agreement is much better between SCIAMACHY and smoothed MLS data than with unsmoothed MLS data. The most striking difference is the significant negative trend in the NH Arctic stratosphere seen in the SCIAMACHY data while MLS shows small positive trends which are not changed by the smoothing.

Figure 21 shows the phase of the annual cycle for collocated data of SCIAMACHY and MLS. Also here, the smaller sample of SCIAMACHY data shows a similar pattern to the results from the time series based on all available data in Fig. 10. Below 15 km the phase of the annual cycle is similar for SCIAMACHY and unsmoothed MLS data. Here, the largest differences can be seen in the tropics. From 15 to 18 km there is usually not more than 1 month difference in the phase of the annual cycle with the exception of SH mid-latitudes and high latitudes, where the patterns start to look different above 15 km. Above 18 km the patterns completely disagree. For MLS the tape recorder effect is clearly visible

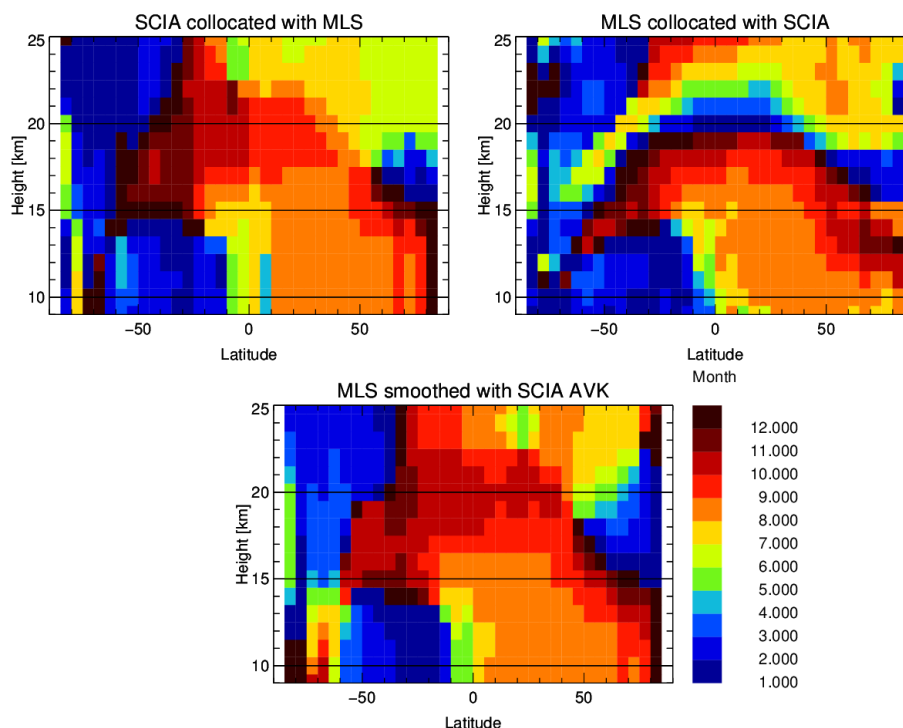


**Figure 21.** Month with the maximum of the annual cycle for zonal monthly mean collocated data from SCIAMACHY and MLS (unsmoothed and smoothed with SCIAMACHY AVKs). Collocations are found between August 2004 and March 2012.

through a phase shift of the annual cycle with increasing altitude for all altitudes in the tropics, for SCIAMACHY this is only the case up to about 18 km. If MLS data are smoothed with SCIAMACHY AVKs, the tape recorder signal above 18 km disappears, demonstrating a clear influence of the vertical resolution on the phase of the annual cycle. Also for most other latitudes the pattern above 18 km is changed by the smoothing and becomes more similar to the pattern for the SCIAMACHY data.

#### 4 Discussions

SCIAMACHY limb water vapour V3.01 agrees well with most other data sets, especially between 14 and 20 km. In this altitude range, the results of the end-to-end tests also show the smallest errors. The retrieval precision for a single profile calculated from the residual of the fit is usually about 10 % in the end-to-end tests (Figs. 3–6) and between 10 and 20 % for measured SCIAMACHY profiles (Fig. 1). The largest errors for the SCIAMACHY profiles are found in the lowest and highest altitudes of the retrieved profile. The error is nearly constant with altitude for the end-to-end tests but not for an observed SCIAMACHY profile. This is because in the simulations a fixed SNR was assumed while in the SCIAMACHY retrieval the SNR depends on the residuals and varies with altitude. The magnitude of the relative errors for SCIAMACHY profiles and its altitude dependence

fits well to the observed differences with the other data sets, where differences are usually below 10 % and smallest in the middle of the profile and increase towards lower and higher altitudes. Above 20 km and below 14 km, differences increase to up to about 30 and 50 % for several instruments, respectively. Differences to HALOE at the lowest altitudes are even larger, but HALOE v19 is known to be rather dry in this region compared with other instruments (Kley et al., 2000; Hegglin et al., 2013).

There are some similar features in the comparison between SCIAMACHY limb water vapour and several other instruments, indicating systematic errors in the SCIAMACHY data. The most obvious one is the difference in the stratosphere above about 20 km outside the tropics which is present and similar in magnitude in nearly all comparisons (see Figs. 13–19). This indicates that there is a possible dry bias in the SCIAMACHY data. Its magnitude is usually around 20 % but varies between different latitude bands. The difference in the comparison to the lunar and solar occultation data is probably mainly due to their location on different hemispheres. The possible dry bias was smaller in the previous data version V3 (Rozanov et al., 2011a). Its increase in V3.01 is most probably related to changes in the aerosol correction. The influence of the aerosol correction can vary with latitude due to the latitudinal variation of the scattering angle, aerosol load, and SNR.

Differences in the comparisons to several data sets indicate a possible wet bias in the tropical SCIAMACHY data below 18 km (Figs. 13 and 16). Outside the tropics, SCIAMACHY is also often wetter in the lowest altitudes compared to some other satellite instruments and the FISH in situ measurements but agrees well with balloon FPH data, MIPAS, and ACE-FTS. The differences in the lower altitudes are partly caused by the higher spatial and temporal variability of the water vapour in the troposphere and near the tropopause which makes comparisons more challenging. Also diurnal effects (e.g. Carminati et al., 2014) can play a role if there is a systematic time difference between the data sets (e.g. Damadeo et al., 2014). This is for example the case for MLS, which usually measures in the afternoon with an equator crossing time of 01:45 LT (Schoeberl et al., 2006; Waters et al., 2006), while the equator crossing time of SCIAMACHY is 10:00 LT (Gottwald and Bovensmann, 2011). In the tropics and SH mid-latitudes, where this difference is found, compared to most other instruments, including balloon data, it indicates a systematic bias in the SCIAMACHY retrieval. This is most probably related to the aerosol correction or the surface elevation retrieval.

It should be noted, that for the profile and time series comparison plots, the other data sets in Figs. 15–19 are already smoothed with the AVK of SCIAMACHY. Therefore, observed differences are not related to the resolution or the shape of the a priori profile. These effects are shown in Figs. 12, 13, 20, and 21 where comparisons are shown for smoothed and non-smoothed data.

Because of the relatively coarse vertical resolution in the upper part of the water vapour profile and because the measurements above about 25 km cannot be used, the SCIAMACHY limb water vapour retrieval fails to detect the tape recorder above about 18 km. The fact that the tape recorder is not observed at higher altitudes was already described in Hegglin et al. (2013). Here, we show that this can be explained completely by the vertical resolution of the SCIAMACHY water vapour profiles, because smoothing the MLS data with the AVK of SCIAMACHY suppresses the tape recorder, too. The coarser resolution for the upper part of the profile has the effect that between the measurement height at about 18.3 and 21.6 km, the influence of the measurements at 18.3 km is dominant. Even at 22 km there is a clear influence from the measurement at 18.3 km (see Fig. 1, middle panel). The SNR for the measurement at about 24.9 km is usually too low; therefore its influence is even smaller than the one from the measurement at 21.6 km. Higher measurement heights are not taken into account at all due to their low SNR.

Therefore, the retrieval result above 19 km is influenced by the measurements at about 18.3 and 21.6 km altitudes, i.e. the measurement at 18.3 km influences all altitudes above because there, the SNR decreases and the smoothing constraint increases. Because the annual cycle is more pronounced at 18.3 km and has a different phase due to the tape recorder,

this leads to a phase shift of the observed annual cycle above 18 km and hence destroys the tape recorder signal in the SCIAMACHY water vapour V3.01.

This clearly demonstrates that the vertical resolution should not be neglected in the data comparison and that derived quantities like the tape recorder signal and the vertical velocity in the stratosphere, which can be calculated from steepness of the tape recorder (e.g. Mote et al., 1996; Niwano et al., 2003; Schoeberl et al., 2008), are affected by the inherent smoothing. The effect is of minor importance for linear trends because they do not show a large change with altitude above 20 km (see Fig. 20).

The coarser resolution at these altitudes is found in the SCIAMACHY limb water vapour retrieval, because of the decreasing SNR in the spectral range used and a stronger regularization needed in the retrieval. Retrieval for other trace gases and the water vapour retrieval from occultation data usually have a higher SNR (e.g. Azam et al., 2012; Rozanov et al., 2011b; von Savigny et al., 2005b). In addition to differences in the retrieval setup and regularization, this implies that their resolution differs from the one of water vapour and does not show necessarily the same decline with increasing altitude. Changes of retrieval grid and regularization can possibly improve the resolution for limb water vapour profiles at these altitudes for future versions of the water vapour retrieval.

After applying the AVKs, some differences in the phase of the annual cycle remain but they are usually much smaller than without smoothing the MLS data with the SCIAMACHY AVK (Fig. 21). In the NH mid-latitudes and high latitudes there is a remaining phase shift of 1 month above 19 km after the smoothing between the annual cycle of SCIAMACHY and MLS; in the tropics, it is up to 2 months (Fig. 21). In the same regions consistent annual cycles are found in the differences between MLS and MIPAS after smoothing (see Figs. 17 and 19). Therefore, there must be additional reasons for these differences, which are not explained by the SCIAMACHY AVKs. Sampling, as e.g. discussed in Damadeo et al. (2014), could play a role in MLS because there is always a latitude-dependent time difference, but it is unlikely in the case of MIPAS, where the time difference is less than half an hour after both instruments measured from Envisat.

Figure 17 shows a possible drift in the differences to MLS and several other instruments, which is most likely explained by the increasing load of volcanic aerosols from 2008 on due to several volcanic eruptions influencing the NH extratropical stratosphere (e.g. Ernst et al., 2012; Trickl et al., 2013). The aerosol correction for the SCIAMACHY water vapour retrieval is apparently not capable of correcting for volcanic aerosols completely. In the end-to-end tests large errors were found for high aerosol loads and volcanic aerosols. The volcanic aerosol simulations indicate that an increased aerosol load as observed in the NH can lead to decreasing water vapour amounts in the upper part of the profile. But the ef-

fects of aerosols on the water vapour retrieval that are not completely corrected depend on the kinds of aerosol and their vertical distribution.

In the tropical lower stratosphere, a significant positive trend is observed by SCIAMACHY between August 2002 and April 2012. A similar trend is also found for collocated data from MLS and SCIAMACHY (during their overlap time starting in August 2004). Figure 19 also shows good agreement and no obvious drifts compared to ACE-FTS, MIPAS, and MLS in the tropics at 18 and 22 km height. Therefore, our study indicates that the increase of water vapour mixing ratios in the tropical lower stratosphere is real. It agrees qualitatively with the increase seen in Urban et al. (2014) as well as with an observed temperature increase in the TTL after 2001 and an increase of water vapour near the stratopause between 2004 and 2013 (Nedoluha et al., 2011). It is beyond the scope of this study to investigate its reasons and longer time series would be necessary to see if the increase continues or if it is a part of a long-term periodic variation. Ongoing time series of water vapour in the tropical UTLS are currently available from MLS and ACE-FTS, but their continuation into the future is uncertain due to the age of these instruments and missing prospects of new limb measurements in the UTLS for a number of trace gases including water vapour. In situ measurements are currently not available globally; there are few measurements in the tropics and few long and consistent ground-based time series only exist at selected NH mid-latitudes (e.g. Hurst et al., 2011; Hegglin et al., 2014; Urban et al., 2014).

## 5 Conclusions

Water vapour profiles are retrieved from SCIAMACHY limb measurements between 10 and 25 km. Considering the resolution and the vertical sampling of the instruments, the results are reliable between about 11 and 23 km. For data version V3.01 data are available during the complete measurement period of SCIAMACHY, from August 2002 to April 2012. To cover the complete time span and due to the long processing time, data were retrieved for every eighth day globally and for every second day between 45° S and 45° N.

The comparison to other data sets and the end-to-end tests show that accuracy of the SCIAMACHY limb water version V3.01 is in the order of 10 % between about 14 and 20 km, if the vertical resolution of the data is taken into account. This is within the retrieval precision of the individual profiles. Above 20 km an accuracy of about 20 % is expected from the end-to-end test and the single profile error. A possible dry bias is found, varying between 0 and 30 % depending on latitude, when compared to other data sets. Below 14 km, larger differences between SCIAMACHY and various data sets occur. Because of the high variability of water vapour and the large differences between data sets near the tropopause, it is unclear if there is a bias in V3.01 at these

altitudes. Most probably, SCIAMACHY limb water vapour V3.01 is rather too wet there, especially in the tropics.

The time series of the SCIAMACHY data set agrees well with the collocated data sets in most regions, indicating a good temporal stability. In the NH stratosphere differences in the annual cycle and linear change are observed compared to several instruments. The differences in the linear change indicate that there is a drift in V3.01 in this region. Its reason is most probably the increasing stratospheric aerosol load in the NH due to more frequent volcanic eruptions after summer 2008. Volcanic aerosols are most probably not covered completely by the current aerosol correction. Therefore, we are working on an improved aerosol correction.

Further improvements are planned for the spectral database of water vapour absorption, tropospheric correction, retrieval grid, regularization, and L1 data version. The last three could together possibly lead to a smaller residual and improve the vertical resolution. This could possibly allow us to detect the tape recorder signal for altitudes above 19 km, which is not possible with the current resolution and altitude coverage of the retrieved water vapour profiles.

The positive trend in the tropical lower stratosphere has been observed by SCIAMACHY and most other instruments (Figs. 19 and 20). In V3.01 the water vapour increases with about 10 % per decade above 20 km between 10° S and 10° N from August 2002 to April 2012. This may be related to changes in the Brewer–Dobson circulation; however, without extending the time series, it is not clear whether this is a continuing trend or only a part of a low frequency variability.

*Acknowledgements.* This work has been supported by the DFG Research Unit FOR 1095 “Stratospheric Change and its role for Climate Prediction (SHARP)” (Project: GZ WE 3647/3-1; www.fu-berlin.de/sharp/) and the ESA Project SPIN (ESA SPARC Initiative). This study has been funded by the DLR Space Agency (Germany), grant 50EE0727, and SADOS (SCIAMACHY algorithm development and operations support), European Commission EC SCOUT-O3, by the University and State of Bremen, and by the SCIAMACHY Quality Working Group Project (ESA). Some data shown here were calculated on the German HLRN (High-Performance Computer Center North). We are thankful to the ECMWF for providing pressure, temperature, and surface elevation information and to the authors of the thread-safe FORTRAN library GALAHAD. The Atmospheric Chemistry Experiment (ACE), also known as SCISAT, is a Canadian-led mission mainly supported by the Canadian Space Agency and the Natural Sciences and Engineering Research Council of Canada. We thank Sam Oltmans and Dale F. Hurst (NOAA Earth System Research Laboratory, Global Monitoring Division) for providing NOAA FPH profile data. Our gratitude also goes to the HALOE science and data processing teams for providing the profiles used in this study. We thank the Karlsruhe Institute of Technology for providing MIPAS water vapour data based on the scientific IMK/IAA processor. The MLS data used in this research were produced by the Jet Propulsion Laboratory, California Institute of Technology, under contract with

the National Aeronautics and Space Administration. Further thanks go to the NASA Langley Research Center (NASA-LaRC) for providing SAGE II data.

The article processing charges for this open-access publication were covered by the University of Bremen.

Edited by: F. Khosrawi

## References

- Azam, F., Bramstedt, K., Rozanov, A., Weigel, K., Bovensmann, H., Stiller, G. P., and Burrows, J. P.: SCIAMACHY lunar occultation water vapor measurements: retrieval and validation results, *Atmos. Meas. Tech.*, 5, 2499–2513, doi:10.5194/amt-5-2499-2012, 2012.
- Backus, G. E. and Gilbert, F. E.: Uniqueness in the inversion of inaccurate gross Earth data, *Philos. T. Roy. Soc. Lond. A*, 266, 123–192, 1970.
- Bernath, P. F., McElroy, C. T., Abrams, M. C., Boone, C. D., Butler, M., Camy-Peyret, C., Carleer, M., Clerbaux, C., Coheur, P.-F., Colin, R., DeCola, P., DeMazière, M., Drummond, J. R., Dufour, D., Evans, W. F. J., Fast, H., Fussen, D., Gilbert, K., Jennings, D. E., Llewellyn, E. J., Lowe, R. P., Mahieu, E., McConnell, J. C., McHugh, M., McLeod, S. D., Michaud, R., Midwinter, C., Nassar, R., Nichitiu, F., Nowlan, C., Rinsland, C. P., Rochon, Y. J., Rowlands, N., Semeniuk, K., Simon, P., Skelton, R., Sloan, J. J., Soucy, M.-A., Strong, K., Tremblay, P., Turnbull, D., Walker, K. A., Walkty, I., Wardle, D. A., Wehrle, V., Zander, R., and Zou, J.: Atmospheric Chemistry Experiment (ACE) mission overview, *Geophys. Res. Lett.*, 32, L15S01, doi:10.1029/2005GL022386, 2005.
- Boone, C. D., Walker, K. A., and Bernath, P. F.: Version 3 retrievals for the Atmospheric Chemistry Experiment Fourier Transform Spectrometer (ACE-FTS), in: *The Atmospheric Chemistry Experiment ACE at 10: A Solar Occultation Anthology*, edited by: Bernath, P. F., A. Deepak Publishing, Hampton, Virginia, USA, 103–127, 2013.
- Bovensmann, H., Burrows, J. P., Buchwitz, M., Frerick, J., Noël, S., Rozanov, V. V., Chance, K. V., and Goede, A. P. H.: SCIAMACHY: mission objectives and measurement modes, *J. Atmos. Sci.*, 56, 127–149, 1999.
- Buchwitz, M., Rozanov, V. V., and Burrows, J. P.: A correlated- $k$  distribution scheme for overlapping gases suitable for retrieval of atmospheric constituents from moderate resolution radiance measurements in the visible/near-infrared spectral region, *J. Geophys. Res.*, 105, 15247–15261, 2000.
- Burrows, J. P., Holzle, E., Goede, A. P. H., Visser, H., and Fricke, W.: SCIAMACHY – SCanning Imaging Absorption spectroMeter for Atmospheric CHartographY, *Acta Astronaut.*, 35, 445–451, 1995.
- Cairo, F., Pommereau, J. P., Law, K. S., Schlager, H., Garnier, A., Fierli, F., Ern, M., Streibel, M., Arabas, S., Borrmann, S., Berthelier, J. J., Blom, C., Christensen, T., D’Amato, F., Di Donfrancesco, G., Deshler, T., Diedhiou, A., Durry, G., Engelsens, O., Goutail, F., Harris, N. R. P., Kerstel, E. R. T., Khaykin, S., Konopka, P., Kylling, A., Larsen, N., Lebel, T., Liu, X., MacKenzie, A. R., Nielsen, J., Oulanowski, A., Parker, D. J., Pelon, J., Polcher, J., Pyle, J. A., Ravegnani, F., Rivière, E. D., Robinson, A. D., Röckmann, T., Schiller, C., Simões, F., Stefanutti, L., Stroh, F., Some, L., Siegmund, P., Sitnikov, N., Vernier, J. P., Volk, C. M., Voigt, C., von Hobe, M., Viciani, S., and Yushkov, V.: An introduction to the SCOUT-AMMA stratospheric aircraft, balloons and sondes campaign in West Africa, August 2006: rationale and roadmap, *Atmos. Chem. Phys.*, 10, 2237–2256, doi:10.5194/acp-10-2237-2010, 2010.
- Carleer, M. R., Boone, C. D., Walker, K. A., Bernath, P. F., Strong, K., Sica, R. J., Randall, C. E., Vömel, H., Kar, J., Höpfner, M., Milz, M., von Clarmann, T., Kivi, R., Valverde-Canossa, J., Sioris, C. E., Izawa, M. R. M., Dupuy, E., McElroy, C. T., Drummond, J. R., Nowlan, C. R., Zou, J., Nichitiu, F., Lossow, S., Urban, J., Murtagh, D., and Dufour, D. G.: Validation of water vapour profiles from the Atmospheric Chemistry Experiment (ACE), *Atmos. Chem. Phys. Discuss.*, 8, 4499–4559, doi:10.5194/acpd-8-4499-2008, 2008.
- Carminati, F., Ricaud, P., Pommereau, J.-P., Rivière, E., Khaykin, S., Attié, J.-L., and Warner, J.: Impact of tropical land convection on the water vapour budget in the tropical tropopause layer, *Atmos. Chem. Phys.*, 14, 6195–6211, doi:10.5194/acp-14-6195-2014, 2014.
- Damadeo, R. P., Zawodny, J. M., Thomason, L. W., and Iyer, N.: SAGE version 7.0 algorithm: application to SAGE II, *Atmos. Meas. Tech.*, 6, 3539–3561, doi:10.5194/amt-6-3539-2013, 2013.
- Damadeo, R. P., Zawodny, J. M., and Thomason, L. W.: Reevaluation of stratospheric ozone trends from SAGE II data using a simultaneous temporal and spatial analysis, *Atmos. Chem. Phys.*, 14, 13455–13470, doi:10.5194/acp-14-13455-2014, 2014.
- Di Pierro, M., Jaeglé, L., Eloranta, E. W., and Sharma, S.: Spatial and seasonal distribution of Arctic aerosols observed by the CALIOP satellite instrument (2006–2012), *Atmos. Chem. Phys.*, 13, 7075–7095, doi:10.5194/acp-13-7075-2013, 2013.
- Dupuy, E., Walker, K. A., Kar, J., Boone, C. D., McElroy, C. T., Bernath, P. F., Drummond, J. R., Skelton, R., McLeod, S. D., Hughes, R. C., Nowlan, C. R., Dufour, D. G., Zou, J., Nichitiu, F., Strong, K., Baron, P., Bevilacqua, R. M., Blumenstock, T., Bodeker, G. E., Borsdorff, T., Bourassa, A. E., Bovensmann, H., Boyd, I. S., Bracher, A., Brogniez, C., Burrows, J. P., Catoire, V., Ceccherini, S., Chabrillat, S., Christensen, T., Coffey, M. T., Cortesi, U., Davies, J., De Clercq, C., Degenstein, D. A., De Mazière, M., Demoulin, P., Dodion, J., Firan-ski, B., Fischer, H., Forbes, G., Froidevaux, L., Fussen, D., Gerard, P., Godin-Beekmann, S., Goutail, F., Granville, J., Griffith, D., Haley, C. S., Hannigan, J. W., Höpfner, M., Jin, J. J., Jones, A., Jones, N. B., Jucks, K., Kagawa, A., Kasai, Y., Kerzenmacher, T. E., Kleinböhl, A., Klekociuk, A. R., Kramer, I., Küllmann, H., Kuttippurath, J., Kyrölä, E., Lambert, J.-C., Livesey, N. J., Llewellyn, E. J., Lloyd, N. D., Mahieu, E., Manney, G. L., Marshall, B. T., McConnell, J. C., McCormick, M. P., McDermid, I. S., McHugh, M., McLinden, C. A., Mellqvist, J., Mizutani, K., Murayama, Y., Murtagh, D. P., Oelhaf, H., Parrish, A., Petelina, S. V., Piccolo, C., Pommereau, J.-P., Randall, C. E., Robert, C., Roth, C., Schneider, M., Senten, C., Steck, T., Strandberg, A., Strawbridge, K. B., Sussmann, R., Swart, D. P. J., Tarasick, D. W., Taylor, J. R., Tétard, C., Thomason, L. W., Thompson, A. M., Tully, M. B., Urban, J., Vanhelle-mont, F., Vigouroux, C., von Clarmann, T., von der Gathen, P.,

- von Savigny, C., Waters, J. W., Witte, J. C., Wolff, M., and Zawodny, J. M.: Validation of ozone measurements from the Atmospheric Chemistry Experiment (ACE), *Atmos. Chem. Phys.*, 9, 287–343, doi:10.5194/acp-9-287-2009, 2009.
- Eichmann, K.-U., von Savigny, C., Reichl, P., Robert, C., Steinwagner, J., Bovensmann, H., and Burrows, J. P.: SCODA: SCIAMACHY Cloud Detection Algorithm from Limb Radiance Measurements – Algorithm theoretical basis document, Tech. rep., Institute of Environmental Physics, University of Bremen, unpublished technical document, 2009.
- Eichmann, K.-U., Lelli, L., von Savigny, C., Sembhi, H., and Burrows, J. P.: Global cloud top height retrieval using SCIAMACHY limb spectra: model studies and first results, *Atmos. Meas. Tech. Discuss.*, 8, 8295–8352, doi:10.5194/amtd-8-8295-2015, 2015.
- Ernst, F., von Savigny, C., Rozanov, A., Rozanov, V., Eichmann, K.-U., Brinkhoff, L. A., Bovensmann, H., and Burrows, J. P.: Global stratospheric aerosol extinction profile retrievals from SCIAMACHY limb-scatter observations, *Atmos. Meas. Tech. Discuss.*, 5, 5993–6035, doi:10.5194/amtd-5-5993-2012, 2012.
- Fischer, H., Birk, M., Blom, C., Carli, B., Carlotti, M., von Clarmann, T., Delbouille, L., Dudhia, A., Ehhalt, D., Endemann, M., Flaud, J. M., Gessner, R., Kleinert, A., Koopman, R., Langen, J., López-Puertas, M., Mosner, P., Nett, H., Oelhaf, H., Perron, G., Remedios, J., Ridolfi, M., Stiller, G., and Zander, R.: MIPAS: an instrument for atmospheric and climate research, *Atmos. Chem. Phys.*, 8, 2151–2188, doi:10.5194/acp-8-2151-2008, 2008.
- Forster, P. M. and Shine, K. P.: Assessing the climate impact of trends in stratospheric water vapor, *Geophys. Res. Lett.*, 29, 1086, doi:10.1029/2001GL013909, 2002.
- Fueglistaler, S. and Haynes, P. H.: Control of interannual and longer-term variability of stratospheric water vapor, *J. Geophys. Res.*, 110, D24108, doi:10.1029/2005JD006019, 2005.
- Gebhardt, C., Rozanov, A., Hommel, R., Weber, M., Bovensmann, H., Burrows, J. P., Degenstein, D., Froidevaux, L., and Thompson, A. M.: Stratospheric ozone trends and variability as seen by SCIAMACHY from 2002 to 2012, *Atmos. Chem. Phys.*, 14, 831–846, doi:10.5194/acp-14-831-2014, 2014.
- Gottwald, M., Hoor, P., Pan, L. L., Randel, W. J., Hegglin, M. I., and Birner, T.: The extratropical upper troposphere and lower stratosphere, *Rev. Geophys.*, 49, RG3003, doi:10.1029/2011RG000355, 2011.
- Gottwald, M. and Bovensmann, H. (Eds.): SCIAMACHY – Exploring the Changing Earth’s Atmosphere, Springer Science + Business Media B. V., Dordrecht, Heidelberg, London, New York, doi:10.1007/978-90-481-9896-2, 2011.
- Gould, N. I. M., Orban, D., and Toint, P. L.: GALAHAD, a library of thread-safe Fortran 90 packages for large-scale nonlinear optimization, *ACM T. Math. Software*, 29, 353–372, doi:10.1145/962437.962438, 2003.
- Groß, J.-U. and Russell III, James M.: Technical note: A stratospheric climatology for O<sub>3</sub>, H<sub>2</sub>O, CH<sub>4</sub>, NO<sub>x</sub>, HCl and HF derived from HALOE measurements, *Atmos. Chem. Phys.*, 5, 2797–2807, doi:10.5194/acp-5-2797-2005, 2005.
- Hegglin, M. I., Boone, C. D., Manney, G. L., Shepherd, T. G., Walker, K. A., Bernath, P. F., Daffer, W. H., Hoor, P., and Schiller, C.: Validation of ACE-FTS satellite data in the upper troposphere/lower stratosphere (UTLS) using non-coincident measurements, *Atmos. Chem. Phys.*, 8, 1483–1499, doi:10.5194/acp-8-1483-2008, 2008.
- Hegglin, M. I., Tegtmeier, S., Anderson, J., Froidevaux, L., Fuller, R., Funke, B., Jones, A., Lingenfelter, G., Lumpe, J., Pendlebury, D., Remsberg, E., Rozanov, A., Toohey, M., Urban, J., von Clarmann, T., Walker, K. A., Wang, R., and Weigel, K.: SPARC Data Initiative: comparison of water vapor climatologies from international satellite limb sounders, *J. Geophys. Res.-Atmos.*, 118, 11824–11846, doi:10.1002/jgrd.50752, 2013.
- Hegglin, M. I., Plummer, D. A., Shepherd, T. G., Scinocca, J. F., Anderson, J., Froidevaux, L., Funke, B., Hurst, D., Rozanov, A., Urban, J., von Clarmann, T., Walker, K. A., Wang, H. J., Tegtmeier, S., and Weigel, K.: Vertical structure of stratospheric water vapour trends derived from merged satellite data, *Nat. Geosci.*, 7, 768–776, doi:10.1038/ngeo2236, 2014.
- Hoffmann, L., Kaufmann, M., Spang, R., Müller, R., Remedios, J. J., Moore, D. P., Volk, C. M., von Clarmann, T., and Riese, M.: Envisat MIPAS measurements of CFC-11: retrieval, validation, and climatology, *Atmos. Chem. Phys.*, 8, 3671–3688, doi:10.5194/acp-8-3671-2008, 2008.
- Hurst, D. F., Oltmans, S. J., Vomel, H., Rosenlof, K. H., Davis, S. M., Ray, E. A., Hall, E. G., and Jordan, A.: Stratospheric water vapor trends over Boulder, Colorado: analysis of the 30 year Boulder record, *J. Geophys. Res.*, 116, D02306, doi:10.1029/2010JD015065, 2011.
- Hurst, D. F., Lambert, A., Read, W. G., Davis, S. M., Rosenlof, K. H., Hall, E. G., Jordan, A. F., and Oltmans, S. J.: Validation of Aura Microwave Limb Sounder stratospheric water vapor measurements by the NOAA frost point hygrometer, *J. Geophys. Res.-Atmos.*, 119, 1612–1625, doi:10.1002/2013JD020757, 2014.
- Khosrawi, F., Urban, J., Lossow, S., Stiller, G., Weigel, K., Braesicke, P., Pitts, M. C., Rozanov, A., Burrows, J. P., and Murtagh, D.: Sensitivity of polar stratospheric cloud formation to changes in water vapour and temperature, *Atmos. Chem. Phys. Discuss.*, 15, 17743–17796, doi:10.5194/acpd-15-17743-2015, 2015.
- Kley, D., Russell III, J. M., and Phillips, C. (Eds.): Assessment of Upper Tropospheric and Stratospheric Water Vapour, SPARC Rep. 2, WMO, TD 1043, World Meteorol. Organ., Geneva, Switzerland, 2000.
- Kneizys, F. X., Shettle, E. P., Abreu, L. W., Chetwynd, J. H., Anderson, G. P., Gallery, W. O., Selby, J. E. A., and Clough, S. A.: Users Guide to LOWTRAN 7, Tech. rep., Air Force Geophysics Laboratory AFGL, Hanscom AFB, Massachusetts, 1986.
- Konopka, P., Günther, G., Müller, R., dos Santos, F. H. S., Schiller, C., Ravegnani, F., Ulanovsky, A., Schlager, H., Volk, C. M., Viciani, S., Pan, L. L., McKenna, D.-S., and Riese, M.: Contribution of mixing to upward transport across the tropical tropopause layer (TTL), *Atmos. Chem. Phys.*, 7, 3285–3308, doi:10.5194/acp-7-3285-2007, 2007.
- Kunz, A., Mueller, R., Homonnai, V., Janosi, I. M., Hurst, D., Rap, A., Forster, P. M., Rohrer, F., Spelten, N., and Riese, M.: Extending water vapor trend observations over Boulder into the tropopause region: trend uncertainties and resulting radiative forcing, *J. Geophys. Res.-Atmos.*, 118, 11269–11284, doi:10.1002/jgrd.50831, 2013.
- Kunz, A., Spelten, N., Konopka, P., Müller, R., Forbes, R. M., and Wernli, H.: Comparison of Fast In situ Stratospheric Hygrometer (FISH) measurements of water vapor in the upper tropo-

- sphere and lower stratosphere (UTLS) with ECMWF (re)analysis data, *Atmos. Chem. Phys.*, 14, 10803–10822, doi:10.5194/acp-14-10803-2014, 2014.
- Lossow, S., Steinwagner, J., Urban, J., Dupuy, E., Boone, C. D., Kellmann, S., Linden, A., Kiefer, M., Grabowski, U., Glatthor, N., Höpfner, M., Röckmann, T., Murtagh, D. P., Walker, K. A., Bernath, P. F., von Clarmann, T., and Stiller, G. P.: Comparison of HDO measurements from Envisat/MIPAS with observations by Odin/SMR and SCISAT/ACE-FTS, *Atmos. Meas. Tech.*, 4, 1855–1874, doi:10.5194/amt-4-1855-2011, 2011.
- Mauldin, L. E., Zaun, N. H., McCormick, M. P., Guy, J. H., and Vaughn, W. R.: Stratospheric Aerosol and Gas Experiment II instrument: a functional description, *Opt. Eng.*, 24, 307–312, doi:10.1117/12.7973473, 1985.
- Meyer, J., Rolf, C., Schiller, C., Rohs, S., Spelten, N., Afchine, A., Zöger, M., Sitnikov, N., Thornberry, T. D., Rollins, A. W., Bozóki, Z., Tátrai, D., Ebert, V., Kühnreich, B., Mackrodt, P., Möhler, O., Saathoff, H., Rosenlof, K. H., and Krämer, M.: Two decades of water vapor measurements with the FISH fluorescence hygrometer: a review, *Atmos. Chem. Phys.*, 15, 8521–8538, doi:10.5194/acp-15-8521-2015, 2015.
- Milz, M., Clarmann, T. v., Bernath, P., Boone, C., Buehler, S. A., Chauhan, S., Deuber, B., Feist, D. G., Funke, B., Glatthor, N., Grabowski, U., Griesfeller, A., Haeefe, A., Höpfner, M., Kämpfer, N., Kellmann, S., Linden, A., Müller, S., Nakajima, H., Oelhaf, H., Remsberg, E., Rohs, S., Russell III, J. M., Schiller, C., Stiller, G. P., Sugita, T., Tanaka, T., Vömel, H., Walker, K., Wetzel, G., Yokota, T., Yushkov, V., and Zhang, G.: Validation of water vapour profiles (version 13) retrieved by the IMK/IAA scientific retrieval processor based on full resolution spectra measured by MIPAS on board Envisat, *Atmos. Meas. Tech.*, 2, 379–399, doi:10.5194/amt-2-379-2009, 2009.
- Mote, P. W., Rosenlof, K. H., McIntyre, M. E., Carr, E. S., Gille, J. C., Holton, J. R., Kinnersley, J. S., Pumphrey, H. C., Russell III, J. M., and Waters, J. W.: An atmospheric tape recorder: the imprint of tropical tropopause temperatures on stratospheric water vapor, *J. Geophys. Res.*, 101, 3989–4006, 1996.
- Naujokat, B.: An update of the observed Quasi-Biennial Oscillation of stratospheric winds over the tropics, *J. Atmos. Sci.*, 43, 1873–1877, 1986.
- Nedoluha, G. E., Michael Gomez, R., Allen, D. R., Lambert, A., Boone, C., and Stiller, G.: Variations in middle atmospheric water vapor from 2004 to 2013, *J. Geophys. Res. Atmos.*, 118, 11285–11293, doi:10.1002/jgrd.50834, 2013.
- Neely III, R. R., English, J. M., Toon, O. B., Solomon, S., Mills, M., and Thayer, J. P.: Implications of extinction due to meteoritic smoke in the upper stratosphere, *Geophys. Res. Lett.*, 38, L24808, doi:10.1029/2011GL049865, 2011.
- Niwano, M., Yamazaki, K., and Shiotani, M.: Seasonal and QBO variations of ascent rate in the tropical lower stratosphere as inferred from UARS HALOE trace gas data, *J. Geophys. Res.*, 108, 4794, doi:10.1029/2003JD003871, 2003.
- Noël, S., Bramstedt, K., Rozanov, A., Bovensmann, H., and Burrows, J. P.: Water vapour profiles from SCIAMACHY solar occultation measurements derived with an onion peeling approach, *Atmos. Meas. Tech.*, 3, 523–535, doi:10.5194/amt-3-523-2010, 2010.
- Purser, R. J. and Huang, H. L.: Estimating effective data density in a satellite retrieval or and objective analysis, *J. Appl. Meteorol.*, 32, 1092–1107, 1993.
- Read, W. G., Lambert, A., Bacmeister, J., Cofield, R. E., Christensen, L. E., Cuddy, D. T., Daffer, W. H., Drouin, B. J., Fetzner, E., Froidevaux, L., Fuller, R., Herman, R., Jarnot, R. F., Jiang, J. H., Jiang, Y. B., Kelly, K., Knosp, B. W., Kovalenko, L. J., Livesey, N. J., Liu, H.-C., Manney, G. L., Pickett, H. M., Pumphrey, H. C., Rosenlof, K. H., Sabounchi, X., Santee, M. L., Schwartz, M. J., Snyder, W. V., Stek, P. C., Su, H., Takacs, L. L., Thurstans, R. P., Vömel, H., Wagner, P. A., Waters, J. W., Webster, C. R., Weinstock, E. M., and Wu, D. L.: Aura Microwave Limb Sounder upper tropospheric and lower stratospheric H<sub>2</sub>O and relative humidity with respect to ice validation, *J. Geophys. Res.*, 112, D24S35, doi:10.1029/2007JD008752, 2007.
- Redelsperger, J.-L., Thorncroft, C. D., Diedhiou, A., Lebel, T., Parker, D. J., and Polcher, J.: African monsoon multidisciplinary analysis, *B. Am. Meteorol. Soc.*, 87, 1739–1746, 2006.
- Remsberg, E. E., Russell III, J. M., and Wu, C.-Y.: An interim reference model for the variability of the middle atmosphere water vapor distribution, *Adv. Space Res.*, 10, 51–64, 1990.
- Riese, M., Ploeger, F., Rap, A., Vogel, B., Konopka, P., Dameris, M., Forster, P., and Foster, P.: Impact of uncertainties in atmospheric mixing on simulated UTLS composition and related radiative effects, *J. Geophys. Res.*, 117, D16305, doi:10.1029/2012JD017751, 2012.
- Rodgers, C. D.: *Inverse Methods for Atmospheric Sounding: Theory and Practice*, World Scientific, River Edge, NJ, USA, 2000.
- Rohs, S., Schiller, C., Riese, M., Engel, A., Schmidt, U., Wetter, T., Levin, I., Nakazawa, T., and Aoki, S.: Long-term changes of methane and hydrogen in the stratosphere in the period 1978–2003 and their impact on the abundance of stratospheric water vapor, *J. Geophys. Res.*, 111, D14315, doi:10.1029/2005JD006877, 2006.
- Rollins, A. W., Thornberry, T. D., Gao, R. S., Smith, J. B., Sayres, D. S., Sargent, M. R., Schiller, C., Kraemer, M., Spelten, N., Hurst, D. F., Jordan, A. F., Hall, E. G., Voemel, H., Diskin, G. S., Podolske, J. R., Christensen, L. E., Rosenlof, K. H., Jensen, E. J., and Fahey, D. W.: Evaluation of UT/LS hygrometer accuracy by intercomparison during the NASA MACPEX mission, *J. Geophys. Res.-Atmos.*, 119, 1915–1935, doi:10.1002/2013JD020817, 2014.
- Rosenlof, K. H., Oltmans, S. J., Kley, D., Russell III, J. M., Chiou, E.-W., Chu, W. P., Johnson, D. G., Kelly, K. K., Michelsen, H. A., Nedoluha, G. E., Remsberg, E. E., Toon, G. C., and McCormick, M. P.: Stratospheric water vapor increases over the past half-century, *Geophys. Res. Lett.*, 28, 1195–1198, doi:10.1029/2000GL012502, 2001.
- Rothman, L., Gordon, I., Barbe, A., Benner, D., Bernath, P., Birk, M., Boudon, V., Brown, L., Campargue, A., Champion, J.-P., Chance, K., Coudert, L., Dana, V., Devi, V., Fally, S., Flaud, J.-M., Gamache, R., Goldman, A., Jacquemart, D., Kleiner, I., Lacome, N., Lafferty, W., Mandin, J.-Y., Massie, S., Mikhailenko, S., Miller, C., Moazzen-Ahmadi, N., Naumenko, O., Nikitin, A., Orphal, J., Perevalov, V., Perrin, A., Predoi-Cross, A., Rinsland, C., Rotger, M., Simeckova, M., Smith, M., Sung, K., Tashkun, S., Tennyson, J., Toth, R., Vandaele, A., and Vander Auwera, J.: The HITRAN 2008 molecular

- spectroscopic database, *J. Quant. Spectrosc. Ra.*, 110, 533–572, doi:10.1016/j.jqsrt.2009.02.013, 2009.
- Rozanov, A., Weigel, K., Bovensmann, H., Dhomse, S., Eichmann, K.-U., Kivi, R., Rozanov, V., Vömel, H., Weber, M., and Burrows, J. P.: Retrieval of water vapor vertical distributions in the upper troposphere and the lower stratosphere from SCIAMACHY limb measurements, *Atmos. Meas. Tech.*, 4, 933–954, doi:10.5194/amt-4-933-2011, 2011a.
- Rozanov, A., Kühl, S., Doicu, A., McLinden, C., Puķite, J., Bovensmann, H., Burrows, J. P., Deutschmann, T., Dorf, M., Goutail, F., Grunow, K., Hendrick, F., von Hobe, M., Hrechanyy, S., Lichtenberg, G., Pfeilsticker, K., Pommereau, J. P., Van Roozendael, M., Stroh, F., and Wagner, T.: BrO vertical distributions from SCIAMACHY limb measurements: comparison of algorithms and retrieval results, *Atmos. Meas. Tech.*, 4, 1319–1359, doi:10.5194/amt-4-1319-2011, 2011b.
- Rozanov, V. V., Buchwitz, M., Eichmann, K.-U., De Beek, R., and Burrows, J. P.: SCIATRAN – a new radiative transfer model for geophysical applications in the 240–2400 nm spectral region: the pseudo-spherical version, *Adv. Space. Res.* 29, 1831–1835, 2002.
- Rozanov, V. V., Rozanov, A. V., Kokhanovsky, A. A., and Burrows, J. P.: Radiative transfer through terrestrial atmosphere and ocean: software package SCIATRAN, *J. Quant. Spectrosc. Ra.*, 133, 13–71, doi:10.1016/j.jqsrt.2013.07.004, 2014.
- Russell III, J. M. and Swider, W.: MAP Summary-Structure and Composition, in: MAP Handbook, 32, edited by: Vincent, R. A., SCOSTEP Secretariat, University of Illinois, Urbana-Champaign, Chicago, Springfield, 1–20, 1991.
- Russell III, J. M., Gordley, L. L., Park, J. H., Drayson, S. R., Hesketh, D. H., Cicerone, R. J., Tuck, A. F., Frederick, J. E., Harries, J. E., and Crutzen, P.: The Halogen Occultation Experiment, *J. Geophys. Res.*, 98, 10777–10797, doi:10.1029/93JD00799, 1993.
- Salazar, V., Renard, J.-B., Hauchecorne, A., Bekki, S., and Berthet, G.: A new climatology of aerosols in the middle and upper stratosphere by alternative analysis of GOMOS observations during 2002–2006, *Int. J. Remote Sens.*, 34, 4986–5029, doi:10.1080/01431161.2013.786196, 2013.
- Schiller, C., Krämer, M., Afchine, A., Spelten, N., and Sitnikov, N.: Ice water content of Arctic, midlatitude and tropical cirrus, *J. Geophys. Res.*, 113, 1807–1816, doi:10.1029/2008JD010342, 2008.
- Schoeberl, M. R., Douglass, A. R., Hilsenrath, E., Bhartia, P. K., Beer, R., Waters, J. W., Gunson, M. R., Froidevaux, L., Gille, J. C., Barnett, J. J., Levelt, P. F., and de Cola, P.: Overview of the EOS Aura Mission, *IEEE T. Geosci. Remote.* 44, 1066–1074, doi:10.1109/TGRS.2005.861950, 2006.
- Schoeberl, M. R., Douglass, A. R., Stolarski, R. S., Pawson, S., Strahan, S. E., and Read, W.: Comparison of lower stratospheric tropical mean vertical velocities, *J. Geophys. Res.*, 113, D24109, doi:10.1029/2008JD010221, 2008.
- Snow, M., Weber, M., Machol, J., Viereck, R., and Richard, E.: Comparison of Magnesium II core-to-wing ratio observations during solar minimum 23/24, *J. Space Weather Space Clim.*, 4, A04, doi:10.1051/swsc/2014001, 2014.
- Solomon, S., Rosenlof, K. H., Portmann, R. W., Daniel, J. S., Davis, S. M., Sanford, T. J., and Plattner, G.-K.: Contributions of stratospheric water vapor to decadal changes in the rate of global warming, *Science*, 327, 1219–1223, 2010.
- Stiller, G. P., Kiefer, M., Eckert, E., von Clarmann, T., Kellmann, S., García-Comas, M., Funke, B., Leblanc, T., Fetzer, E., Froidevaux, L., Gomez, M., Hall, E., Hurst, D., Jordan, A., Kämpfer, N., Lambert, A., McDermid, I. S., McGee, T., Miloshevich, L., Nedoluha, G., Read, W., Schneider, M., Schwartz, M., Straub, C., Toon, G., Twigg, L. W., Walker, K., and Whiteman, D. N.: Validation of MIPAS IMK/IAA temperature, water vapor, and ozone profiles with MOHAVE-2009 campaign measurements, *Atmos. Meas. Tech.*, 5, 289–320, doi:10.5194/amt-5-289-2012, 2012.
- Trickl, T., Giehl, H., Jäger, H., and Vogelmann, H.: 35 yr of stratospheric aerosol measurements at Garmisch-Partenkirchen: from Fuego to Eyjafjallajökull, and beyond, *Atmos. Chem. Phys.*, 13, 5205–5225, doi:10.5194/acp-13-5205-2013, 2013.
- Urban, J., Lossow, S., Stiller, G., and Read, W.: Another drop in water vapour, *EOS T. Am. Geophys. Un.*, 95, 245–252, 2014.
- Van Roozendael, M. and Kalb, N. (Eds.): SPIN Final Report, to be published at: <http://esa-spin.org/index.php/documents>, 2015.
- Vernier, J.-P., Thomason, L. W., Pommereau, J.-P., Bourassa, A., Pelon, J., Garnier, A., Hauchecorne, A., Blanot, L., Trepte, C., Degenstein, D., and Vargas, F.: Major influence of tropical volcanic eruptions on the stratospheric aerosol layer during the last decade, *Geophys. Res. Lett.*, 38, L12807, doi:10.1029/2011GL047563, 2011.
- von Clarmann, T.: Validation of remotely sensed profiles of atmospheric state variables: strategies and terminology, *Atmos. Chem. Phys.*, 6, 4311–4320, doi:10.5194/acp-6-4311-2006, 2006.
- von Clarmann, T., Höpfner, M., Kellmann, S., Linden, A., Chauhan, S., Funke, B., Grabowski, U., Glatthor, N., Kiefer, M., Schieferdecker, T., Stiller, G. P., and Versick, S.: Retrieval of temperature, H<sub>2</sub>O, O<sub>3</sub>, HNO<sub>3</sub>, CH<sub>4</sub>, N<sub>2</sub>O, ClONO<sub>2</sub> and ClO from MIPAS reduced resolution nominal mode limb emission measurements, *Atmos. Meas. Tech.*, 2, 159–175, doi:10.5194/amt-2-159-2009, 2009.
- von Hobe, M., Bekki, S., Borrmann, S., Cairo, F., D’Amato, F., Di Donfrancesco, G., Dörnbrack, A., Ebersoldt, A., Ebert, M., Emde, C., Engel, I., Ern, M., Frey, W., Genco, S., Griensbach, S., Grooß, J.-U., Gulde, T., Günther, G., Hösen, E., Hoffmann, L., Homonnai, V., Hoyle, C. R., Isaksen, I. S. A., Jackson, D. R., Jánosi, I. M., Jones, R. L., Kandler, K., Kalicinsky, C., Keil, A., Khaykin, S. M., Khosrawi, F., Kivi, R., Kuttippurath, J., Laube, J. C., Lefèvre, F., Lehmann, R., Ludmann, S., Luo, B. P., Marchand, M., Meyer, J., Mitev, V., Molleker, S., Müller, R., Oelhaf, H., Olschewski, F., Orsolini, Y., Peter, T., Pfeilsticker, K., Piesch, C., Pitts, M. C., Poole, L. R., Pope, F. D., Ravagnani, F., Rex, M., Riese, M., Röckmann, T., Rognerud, B., Roiger, A., Rolf, C., Santee, M. L., Scheibe, M., Schiller, C., Schlager, H., Siciliani de Cumis, M., Sitnikov, N., Søvde, O. A., Spang, R., Spelten, N., Stordal, F., Sumińska-Ebersoldt, O., Ulanovski, A., Ungermann, J., Viciani, S., Volk, C. M., vom Scheidt, M., von der Gathen, P., Walker, K., Wegner, T., Weigel, R., Weinbruch, S., Wetzela, G., Wienhold, F. G., Wohltmann, I., Woiwode, W., Young, I. A. K., Yushkov, V., Zobrist, B., and Stroh, F.: Reconciliation of essential process parameters for an enhanced predictability of Arctic stratospheric ozone loss and its climate interactions (RECONCILE): activities and results, *Atmos.*

- Chem. Phys., 13, 9233–9268, doi:10.5194/acp-13-9233-2013, 2013.
- von Savigny, C., Ulasi, E. P., Eichmann, K.-U., Bovensmann, H., and Burrows, J. P.: Detection and mapping of polar stratospheric clouds using limb scattering observations, *Atmos. Chem. Phys.*, 5, 3071–3079, doi:10.5194/acp-5-3071-2005, 2005a.
- von Savigny, C., Rozanov, A., Bovensmann, H., Eichmann, K.-U., Noël, S., Rozanov, V. V., Sinnhuber, B.-M., Weber, M., and Burrows, J. P.: The ozone hole break-up in September 2002 as seen by SCIAMACHY on ENVISAT, *J. Atmos. Sci.*, 62, 721–734, 2005b.
- Waters, J., Froidevaux, L., Harwood, R. S., Jarnot, R. F., Pickett, H. M., Read, W. G., Siegel, P. H., Cofield, R. E., Filipiak, M. J., Flower, D. A., Holden, J. R., Lau, G. K., Livesey, N. J., Manney, G. L., Pumphrey, H. C., Santee, M. L., Wu, D. L., Cuddy, D. T., Lay, R. R., Loo, M. S., Perun, V. S., Schwartz, M. J., Stek, P. C., Thurstans, R. P., Boyles, M. A., Chandra, K. M., Chavez, M. C., Chen, G. S., Chudasama, B. V., Dodge, R., Fuller, R. A., Girard, M. A., Jiang, J. H., Jiang, Y. B., Knosp, B. W., LaBelle, R. C., Lam, J. C., Lee, K. A., Miller, D., Oswald, J. E., Patel, N. C., Pukala, D. M., Quintero, O., Scaff, D. M., Van Snyder, W., Tope, M. C., Wagner, P. A., and Walch, M. J., The Earth Observing System Microwave Limb Sounder (EOS MLS) on the Aura satellite, *IEEE T. Geosci. Remote*, 44, 1075–1092, 2006.
- Waymark, C., Walker, K., Boone, C. D., and Bernath, P. F.: ACE-FTS version 3.0 data set: validation and data processing update, *Ann. Geophys.*, 56, 1395–1427, doi:10.4401/ag-6339, 2013.
- Weatherhead, E. C., Reinsel, G. C., Tiao, G. C., Meng, X.-L., Choi, D., Cheang, W.-K., Keller, T., DeLuisi, J., Wuebbles, D. J., Kerr, J. B., Miller, A. J., Oltmans, S. J., and Frederick, J. E.: Factors affecting the detection of trends: statistical considerations and applications to environmental data, *J. Geophys. Res.*, 103, 17149–17161, doi:10.1029/98JD00995, 1998.
- Weber, M., Pagaran, J., Dikty, S., von Savigny, C., Burrows, J. P., DeLand, M., Floyd, L. E., Harder, J. W., Mlynczak, M. G., and Schmidt, H.: Investigation of solar irradiance variations and their impact on middle atmospheric ozone, chapter 3, in: *Climate and Weather of the Sun-Earth System (CAWSES): Highlights from a Priority Program*, edited by: Lübken, F.-J., Springer, Dordrecht, the Netherlands, 2013.
- Weinstock, E. M., Smith, J. B., Sayres, D. S., Pittman, J. V., Spackman, J. R., Hints, E. J., Hanisco, T. F., Moyer, E. J., St. Clair, J. M., Sargent, M. R., and Anderson, J. G.: Validation of the Harvard Lyman- $\alpha$  in situ water vapor instrument: implications for the mechanisms that control stratospheric water vapor, *J. Geophys. Res.*, 114, D23301, doi:10.1029/2009JD012427, 2009.
- Zoeger, M., Afchine, A., Eicke, N., Gerhard, M.-T., Klein, E., McKenna, D. S., Moerschel, U., Schmidt, U., Tan, V., Tuitjer, F., Woyke, T., and Schiller, C.: Fast in situ stratospheric hygrometers: a new family of balloon-borne and airborne Lyman photofragment fluorescence hygrometers, *J. Geophys. Res.*, 105, 1807–1816, 1999.